The American Journal of Pathology, Vol. 178, No. 4, April 2011

DOI: 10.1016/j.ajpath.2010.12.045

Tumorigenesis and Neoplastic Progression

Distinct Profiles of Epigenetic Evolution between Colorectal Cancers with and without Metastasis

Hai-xing Ju,*† Byonggu An,* Yasuyuki Okamoto,* Keiko Shinjo,*‡ Yukihide Kanemitsu,§ Koji Komori,§ Takashi Hirai,§ Yasuhiro Shimizu,§ Tsuyoshi Sano,§ Akira Sawaki,¶ Masahiro Tajika,¶ Kenji Yamao,¶ Makiko Fujii,* Hideki Murakami,* Hirotaka Osada,*‡ Hidemi Ito,‖ Ichiro Takeuchi,** Yoshitaka Sekido,*‡ and Yutaka Kondo*

From the Divisions of Molecular Oncology and Epidemiology and Prevention,‖ Aichi Cancer Center Research Institute, Nagoya, Japan; the Department of Colorectal Surgery,† Zhejiang Cancer Hospital, Hangzhou, China; the Department of Cancer Genetics,‡ Program in Function Construction Medicine, Nagoya University Graduate School of Medicine, Nagoya, Japan; the Departments of Gastroenterological Surgery§ and Gastroenterology,¶ Aichi Cancer Center Central Hospital, Nagoya, Japan; and the Department of Scientific and Engineering Simulation,** Graduate School of Engineering, Nagoya Institute of Technology, Nagoya, Japan*

Liver metastasis is a fatal step in the progression of colorectal cancer (CRC); however, the epigenetic evolution of this process is largely unknown. To decipher the epigenetic alterations during the development of liver metastasis, the DNA methylation status of 12 genes, including 5 classical CpG island methylator phenotype (CIMP) markers, was analyzed in 62 liver metastases and in 78 primary CRCs (53 stage I–III; 25 stage IV). Genome-wide methylation analysis was also performed in stage I–III CRCs and in paired primary and liver metastatic cancers. Methylation frequencies of *MGMT* and *TIMP3* increased progressively from stage I–III CRCs to liver metastasis ($P = 0.043$ and $P = 0.028$, respectively). The CIMP-positive cases showed significantly earlier recurrence of disease than did CIMP-negative cases with liver metastasis ($P = 0.030$), whereas no such difference was found in stage I–III CRCs. Genome-wide analysis revealed that more genes were methylated in stage I–III CRCs than in paired stage IV samples ($P = 0.008$). Hierarchical cluster analysis showed that stage I–III CRCs and stage IV CRCs were clustered into two distinct subgroups, whereas most paired primary and metastatic cancers showed similar methylation profiles. This analysis revealed distinct methylation profiles between stage I–III CRCs and stage IV CRCs, which may reflect differences in epigenetic evolution during progression of the disease. In addition, most methylation status in stage IV CRCs seems to be established before metastasis. ***(Am J Pathol 2011, 178:1835–1846; DOI: 10.1016/j.ajpath.2010.12.045)***

Colorectal cancer (CRC) is one of the most aggressive types of cancer, and it occurs at a high incidence in most countries.[1] Despite several advances in diagnosis and treatment of CRC, the overall survival rate has changed little in the past decade. A major reason is the high occurrence of distant metastasis, the liver being the most common site. As many as 25% of patients with CRC present with liver metastases at the time of diagnosis, and approximately 50% of patients who undergo radical resection for primary CRC are affected by metastatic disease in the liver in the first couple of years after surgery, probably owing to the existence of micrometastasis when the primary tumor is resected.[2,3] Although there have been recent advances in chemotherapy of colorectal liver metastasis, treatment options for patients with advanced disease are limited to only a subset of cases because not all patients are eligible for curative surgical resection, which makes the prognosis of this disease poor.[4,5] A multidisciplinary effort is required to elucidate better means to overcome the current limitations of surgical, chemotherapeutic, and radiotherapeutic intervention.[3] Therefore, understanding the molecular mechanisms underlying metastasis in CRC is important and may, in turn, foster the development of potent therapeutic strategies to combat this disease.

Supported by grants-in-aid for cancer research from the Ministry of Health, Labor, and Welfare; by a grant from the Japan Society for the Promotion of Science, the Japanese Society of Gastroenterology, and the Sagawa Foundation for Promotion of Cancer Research; and by a Japan-China Sasakawa Medical Fellowship (H.J.).

Accepted for publication December 14, 2010.

None of the authors disclosed any relevant financial relationships.

Supplemental material for this article can be found at *http://ajp.amjpathol.org* or at doi:10.1016/j.ajpath.2010.12.045.

Address reprint requests to Yutaka Kondo, M.D., Ph.D., Division of Molecular Oncology, Aichi Cancer Center Research Institute, 1-1 Kanokoden, Chikusa-ku, Nagoya 464-8681, Japan. E-mail: ykondo@aichi-cc.jp.

Cancer progression to metastasis has been thought to occur through clonal genomic and epigenetic evolution.[6–8] Liver metastasis from primary CRC involves a multistep process that is tightly regulated and may require a cancer cell to express genes associated with proteolysis of local extracellular matrix attachments, adhesive alterations, angiogenesis, viable vascular dissemination, distant embolization, and survival in a new environment.[9,10] In this context, a variety of molecular factors have been investigated. Matrix metalloproteinase 7 is involved in proteolysis of the extracellular matrix.[11] Osteopontin mediates anchorage-independent growth, cell adhesion, and cell invasion.[12,13] Vascular endothelial growth factor is a well-known angiogenic factor that stimulates endothelial migration, proliferation, proteolytic activity, and capillary morphogenesis.[14] The expression of these genes is linked to advancing tumor stage, making them potential markers for assessing the risk of liver metastasis.[15] However, not all of these genetic alterations occur during the process of liver metastasis, with other molecular mechanisms potentially being involved.[8,9,16]

DNA hypermethylation, an important epigenetic mechanism, has been reported in many cancers. It can affect multiple cellular processes, including proliferation and apoptosis, by silencing tumor suppressor genes.[17,18] To date, studies have demonstrated that various genes are hypermethylated and associated with tumor progression.[6,9,13,16] A high frequency of *p16/INK4A* methylation has been suggested in stage IV CRC.[19] Hypermethylation of tissue inhibitor of metalloproteinase 3 (*TIMP3*), which encodes for an extracellular matrix–bound protein, in breast cancer is associated with high tumor grade and lymph node metastasis.[20] Aberrant promoter methylation of *RASSF1A* has been linked to progression of nasopharyngeal carcinoma.[21] Recent studies suggested that a subset of CRCs has a unique hypermethylation phenotype, termed CpG island methylator phenotype (CIMP).[22] Tumors affected by this phenotype are characterized by a high degree of concordant CpG island methylation and exhibit characteristic clinicopathologic and molecular features.[23,24] However, only a limited number of genes have been examined in this respect in paired primary and metastatic tumors, and no data are available regarding the global profile of DNA methylation during the process of liver metastasis.

In this study, we examined global DNA methylation status in stage I–III CRCs and in paired primary and metastatic tumors using a methylated CpG island amplification microarray (MCAM) approach; this technique provides reproducible results with a high validation rate and successfully detects genes that are methylated in cancerous tissues.[25–29] Several genes, including five classical CIMP markers, were further examined by quantitative DNA methylation analysis in CRCs and liver metastases. We found characteristic methylation profiles for stage I–III CRCs and stage IV CRCs, which likely reflects different pathologic processes underlying stage IV CRCs compared with stage I–III CRCs. The DNA methylation pattern along a genome is generally inherited faithfully during mitosis, with it potentially being subject to evolution by natural selection during acquisition of the metastatic phenotype. This study sheds light on the underlying mechanisms associated with epigenetic regulation and provides evidence to clarify the nature of epigenetic evolution during progression to metastasis.

Table 1. Backgrounds of Cases with Stage I–III CRCs, Stage IV CRCs, and Liver Metastases

	Stage I–III CRC (n = 53)	Stage IV CRC (n = 25)	Liver metastasis (n = 62)
Age, mean ± SD, years	64.7 ± 9.2	62.1 ± 8.4	62.8 ± 9.8
Sex, No. (%)			
Female	21 (40)	6 (24)	18 (29)
Male	32 (60)	19 (76)	44 (71)
Tumor location, No. (%)*			
Proximal	17 (32)	12 (48)	21 (34)
Distal	36 (68)	13 (52)	41 (66)
Stage, No. (%)			
I	6 (11)	NA	NA
II	25 (47)	NA	NA
III	22 (42)	NA	NA
Pathology, No. (%)†			
Well	4 (8)	2 (8)	3 (6)
Moderately	46 (87)	21 (84)	44 (86)
Poorly	3 (6)	2 (8)	4 (8)
Metastasis period, No. (%)			
Synchronous	NA	NA	25 (40)
Metachronous	NA	NA	37 (60)

NA, not applicable.
*Proximal primary tumors were located in the cecum and the ascending and transverse colon; distal primary tumors were located in the descending and sigmoid colon and the rectum.
†Pathologic findings are available in only 51 cases of liver metastasis.

Material and Methods

Tissue Samples

We collected 78 primary CRC (53 stage I–III and 25 stage IV) and 62 liver metastasis tissue samples from patients who underwent surgical resection at the Aichi Cancer Center Central Hospital, Nagoya, Japan, between January 1, 2006, and December 31, 2008. Tumors were selected solely on the basis of availability during the period. Samples and clinical data were collected after appropriate approval of the Aichi Cancer Center review board was received and written informed consent had been obtained from all the patients. The backgrounds of examined cases are given in Table 1. Pathologic TNM classification was determined according to the criteria of the International Union Against Cancer.[30] Tissue samples were flash frozen and stored at −80°C until analyses. The specimens examined showed a high proportion (>80%) of cancer cells without definite evidence of necrosis. Genomic DNA was extracted using a standard phenol-chloroform method. Regarding the metastasis period, synchronous liver metastasis was defined as metastasis that occurred within 6 months of resection of the primary CRC; metachronous liver metastasis was defined as metastasis that was noted more than 6 months after resection of the primary CRC.[31]

Table 2. Primer Sets for Pyrosequencing Methylation Analysis, MSP, and RT-PCR

Gene*	Primers†	Annealing temperature (°C)	No. of CpGs	Sequencing primers
Primer sequences for pyrosequencing analysis				
RASSF1A (+268 ~ +565)	F: 5′-GGGGGAGTTTGAGTTTATTGA-3′ R: 5′-biotin-CTACCCCTTAACTACCCCTTCC-3′	55	3	5′-GATTTTATTTGGGG-3′
CDH1 (+9 ~ +116)	F: 5′-GGAATTGTAAAGTATTTGTGAGTTT-3′ R: 5′-U-TCCAAAAACCCATAACTAACC-3′	55	2	5′-GGAAGTTAGTTTAGATTTTA-3′
MGMT (−357 ~ −200)	F: 5′-TTGGTAAATTAAGGTATAGAGTTTT-3′ R: 5′-biotin-AAACAATCTACGCATCCT-3′	60/57/54/51	3	5′-GGAAGTTGGGAAGG-3′
TIMP3 (+540 ~ +798)	F: 5′-TTTTGGTTTGGGTTAGAGATAT-3′ R: 5′-U-CCCCCTCAAACCAATAAC-3′	55	2	5′-GTTTTTTTTTTGGAG-3′
hMLH1 (−105 ~ +152)	F: 5′-TTGATTGGTATTTAAGTTGTTTAATT-3′ R: 5′-biotin-CCAATTCTCAATCATCTCTTTAATA-3′	58/56/54/52	2	5′-AGTTATAGTTGAAGGAAGAA-3′
MINT1	F: 5′-GGTTTTTTGTTAGYGTTTGTATTT-3′ R: 5′-biotin-ATTAATCCCTCTCCCCTCTAAACTT-3′	55	3	5′-TTTAGTAAAAATTTTTTGGG-3′
MINT2	F: 5′-AGTGTTAGAAAAATGTGTTG-3′ R: 5′-biotin-CTACAATTAAACATCAATTATAT-3′	50/48/46/44	2	5′-GAATTTTAGTATTTAAGTT-3′
MINT31	F: 5′-TGGTTTTAGTAAAGTGAGGG-3′ R: 5′-biotin-AACCTAATAAATCACTCAATTC-3′	55	3	5′-TGGTGATGGAGGTTATT-3′
P16 (+263 ~ +95)	F: 5′-GGTTGTTTTYGGTTGGTGTTTT-3′ R: 5′-biotin-ACCCTATCCCTCAAATCCTCTAAAA-3′	58/56/54/52	2	5′-GGAGTTAATAGTATTTTT-3′
ANK1 (+211 ~ +370)	F: 5′-TGAGGTGAGTTAGTTAGTTTTAGTTG-3′ R: 5′-U-AATAACCCCCTCCTAACATCTC-3′	60	2	5′-TTTTTTAAGTTTTTAAGGTT-3′
UPK3A (−274 ~ −203)	F: 5′-U-AGGGTTGTTTTGGTTTGGGTATA-3′ R: 5′-AATCCCACCRAACAAAACCTTCT-3′	68/66/64/62	2	5′-AACAAAACCTTCTCCAAC-3′
CYBRD1 (+439 ~ +565)	F: 5′-U-TTTGGGGYGGGATAGAGTTG-3′ R: 5′-CRCCRCAAAAAATTAACCA-3′	58	3	5′-AAAAATTAACCAAATAAAAC-3′
ARAF (−1 ~+153)	F: 5′-U-AGGAGGYGGATTTTGTGAGGAAATA-3′ R: 5′-ACCCAAACRCAACCATCCT-3′	58	2	5′-CCATCCTAAAACTAAACTTT-3′
Primer Sequences for MSP				
ANK1				
Methylated (−205 ~ −37)	F: 5′-TTCGGGGTAATTAGGGGTTC-3′ R: 5′-CCTTATCGACCCCAAAAACG-3′	68/66/64/62	NA	NA
Unmethylated (−207 ~ +19)	F: 5′-ATTTTGGGGTAATTAGGGGTTT-3′ R: 5′-CAAACTCACCACAACCTCTACAA-3′	68/66/64/62	NA	NA
CYBRD1				
Methylated (−40 ~ +132)	F: 5′-TAGTTTTAAGAAGTCGACGTTTC-3′ R: 5′-AAAACCGACGAACAATACCG-3′	62/60/58/55	NA	NA
Unmethylated (−52 ~ +132)	F: 5′-GTAGGTGGAGATAGTTTTAAGAAGTTG-3′ R: 5′-AAAAACCAACAAACAATACCA-3′	62/60/58/55	NA	NA
Primer Sequences for RT-PCR				
UPK3A	F: 5′-TCGGCTGCCTGCGGT-3′ R: 5′-AGAGAGGCTTTTCCAAGGCC-3′	55		NA

F, forward; R, reverse; NA, not applicable.
*The primer location relative to the transcription start site (obtained from the University of California at Santa Cruz Genome Database, version hg17, May 2004) of each gene is indicated in parentheses.
†U indicates the universal primer sequence: biotin-GGGACACCGCTGATCGTTTA.

Cell Lines

Six colon cell lines (SW48, SW480, LS174T, SW1083, RKO, and Lovo) and one hepatocellular carcinoma cell line (Huh7) were used for the study. The colon cell lines were obtained from the American Type Culture Collection (Rockville, MD) or the Japanese Collection of Research Bioresources (Osaka, Japan) and were cultured according to the relevant instructions. Huh7 was the kind gift of Dr. Tetsuro Suzuki (National Institute of Infectious Diseases, Tokyo, Japan). Cell lines were grown in Dulbecco's modified Eagle's medium (Sigma-Aldrich, St. Louis, MO) supplemented with 10% fetal bovine serum (Invitrogen, Carlsbad, CA) and antibiotic-antimycotic (Invitrogen) at 37°C in a humidified incubator with 5% CO_2. Cells were treated with 5-aza-2′-deoxycytidine (Sigma-Aldrich; 1 μmol/L for 72 hours) as described previously.[26]

Quantitative RT-PCR Analyses

Total RNA was isolated using TRIzol (Invitrogen). Two micrograms of RNA was reverse transcribed using Moloney murine leukemia virus (Promega, Madison, WI). Quantitative TaqMan and SYBR Green RT-PCR (Applied Biosystems, Foster City, CA) were performed in triplicate for the target genes of interest. Primer sequences are shown in Table 2.

DNA Methylation Analysis

We performed bisulfite treatment as reported previously.[26] Briefly, 2 μg of genomic DNA was incubated with 3M sodium bisulfite (pH 5.0) for 16 hours at 50°C. DNA was purified using the Wizard DNA purification resin (Promega, Milano, Italy) and was resuspended in 30 μL of diluted water. Conventional methylation-specific PCR (MSP) was performed for the ankyrin 1 gene (*ANK1*) and cytochrome b reductase 1 gene (*CYBRD1*). The PCR products were visualized on 3% agarose gels stained with ethidium bromide. The MSP products were subsequently confirmed by bisulfite sequencing analysis. DNA methylation levels were also measured via a quantitative method using pyrosequencing technology, with 12 methylation markers, including 5 classical CIMP markers (*P16*, *hMLH1*, *MINT1*, *MINT2,* and *MINT31*), being assessed (Pyrosequencing AB, Uppsala, Sweden).[26] The PCR conditions and the main and sequencing primers for amplification of the 12 genes assessed are given in Table 2. Each assay included positive controls (samples after SssI

treatment; New England Biolabs, Ipswich, MA) and negative controls (samples after whole genome amplification using GenomiPhi V2; GE Healthcare, Piscataway, NJ), with mixing experiments to rule out bias and repeated experiments to assess reproducibility. Optimization of annealing temperature for PCR amplification was used to overcome PCR bias.[26] The methylation levels at different C sites, as measured by pyrosequencing, were averaged to represent the degree of methylation in each sample for each gene. Methylation status was analyzed as a continuous variable (methylation level) and as a categorical variable (methylation positive or negative). Genes with methylation levels greater than 15% were considered methylation positive because lower values could not be easily distinguished from background.[28,32]

MCAM Analysis

The MCAM analysis was performed using DNA from eight stage I–III CRCs and nine stage IV CRCs, along with their paired liver metastases and corresponding normal colon mucosa samples (controls). The backgrounds of cases examined by MCAM analysis are shown in Supplemental Table S1 at *http://ajp.amjpathol.org*. A detailed protocol for MCAM analysis has been described previously.[25,26] Herein, we used a human custom promoter array (G4413A; Agilent Technologies, Santa Clara, CA) containing 15,134 probes corresponding to 6157 unique genes, which we had initially validated by the MCAM method in a previous study.[26,28] After hybridization and washing according to the manufacturer's protocol, arrays were scanned using an Agilent scanner and were analyzed using Feature Extraction software; then, data normalization was performed using a linear per-array algorithm according to the manufacturer's protocol (Agilent Technologies). To determine the criteria for the identification of hypermethylated loci, five selected genes [*p16*, O-6-methylguanine-DNA methyltransferase (*MGMT*), *ARAF*, *CYBRD1,* and uroplakin 3A (*UPK3A*)] were subsequently assessed by pyrosequencing analysis in primary CRC and metastasis samples (genes with methylation levels >15% were considered methylation positive). A high concordance was observed between the methylation status as determined by MCAM and pyrosequencing analyses (specificity, 98.8%; sensitivity, 66.7%; and false discovery rate, 0.067; data not shown), as has been demonstrated in previous studies.[25,26,28] Thus, we considered a signal ratio greater than 2.0 via MCAM analysis to be methylation positive.

Hierarchical Clustering Analysis

Cluster analysis was performed using an agglomerative hierarchical clustering algorithm.[28,33] For specimen clustering, pairwise similarity measures among specimens were calculated using statistical software [Cluster 3.0 (*http://rana.lbl.gov/EisenSoftware.htm*) or Minitab 15 (Custom Solutions, Summerville, SC)] based on DNA methylation intensity measurements obtained across all genes assessed.

Statistical Analysis

All statistical analyses were performed using a software program [GraphPad Prism version 4.0 (GraphPad Software, San Diego, CA) or STATA version 11 (StataCorp LP, College Station, TX)]. Differences in clinicopathologic variables were analyzed using Fisher's exact test. Differences in DNA methylation were calculated using the *U*-test or the Kruskal-Wallis test. All reported *P* values were two sided, and $P < 0.05$ was considered statistically significant. Relapse-free survival (RFS) was calculated starting from the date of the surgical procedure to the date of finding new liver metastatic lesions or local recurrences from primary CRC. Survival curves were generated via the Kaplan-Meier method, and the log-rank test was used for statistical analysis. A multivariate analysis using the Cox proportional hazards model was performed for estimation of hazard ratio. The factors considered in the multivariate model included stage and CIMP status, which were marginally ($P < 0.1$) or statistically ($P < 0.05$) significant by Fisher's exact test, in addition to age and sex. All the variables for the multivariate analysis were categorical variables. Patients were observed until the incidence of recurrence after surgery or until September 2008, whichever came first. There were 14 and 26 recurrent cases in stage I–III CRCs and liver metastases, respectively. Median follow-up was 22 months in stage I–III CRCs and 14 months in liver metastases.

Results

Quantitative Methylation Analysis of Nine Candidate Genes in Stage I–III CRCs, Stage IV CRCs, and Liver Metastases

DNA methylation status was examined by pyrosequencing analysis in 53 stage I–III CRCs, 25 stage IV CRCs, and 62 liver metastases (Figure 1 and Table 3). There were no significant differences in terms of age, sex, and tumor location among the three study groups. We examined DNA methylation of five classical CIMP markers because it remains to be understood how CIMP affects the process of liver metastasis despite numerous studies showing its characteristic clinicopathologic and molecular features.[23,24] In addition, we examined the DNA methylation status of *MGMT, RASSF1A, TIMP3,* and *E-cadherin* (*CDH1*) because methylation of each of these genes has already been studied in metastatic CRCs.[19,34,35]

The median DNA methylation level seems to be similar among the three groups (Figure 1). No evidence of substantial DNA methylation of *CDH1* was seen with any of the three groups or with normal colon mucosae. We found that a subset of stage IV CRCs and of liver metastases cases showed a prominently high level of DNA methylation (>80%) in *MGMT*. In addition, some liver metastases showed increased DNA methylation of *TIMP3*, which encodes an inhibitor of the matrix metalloproteinases.

The frequency of positive cases with DNA methylation of the five classical CIMP markers and *RASSF1A* was not

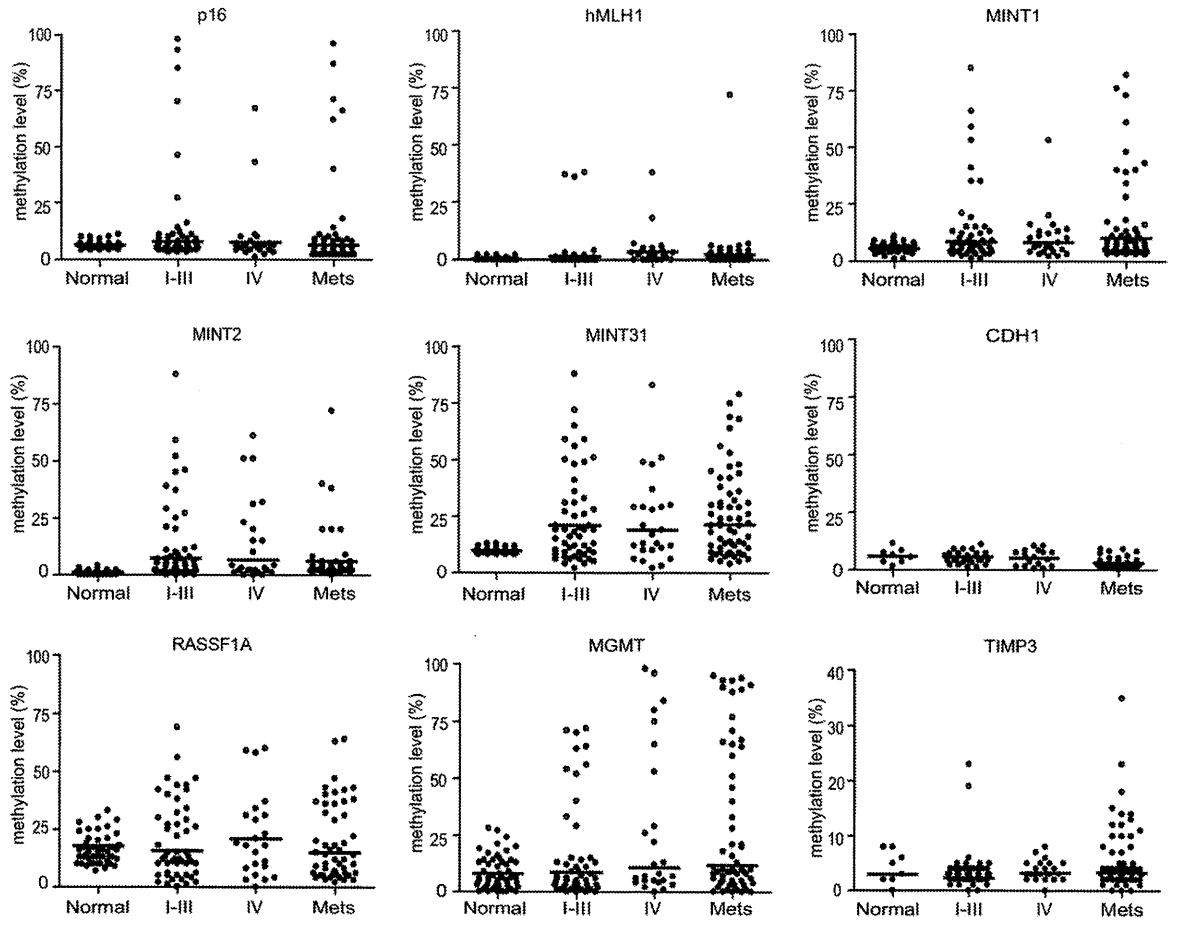

Figure 1. DNA methylation status of nine genes (*p16, hMLH1, MINT1, MINT2, MINT31, CDH1, RASSF1A, MGMT,* and *TIMP3*) in 53 stage I–III CRCs (I–III), 25 stage IV CRCs (IV), and 62 liver metastases (Mets) and corresponding normal colonic mucosae. The *y* axis indicates the level of DNA methylation of each gene, as measured by bisulfite pyrosequencing–based methylation analysis. Each dot represents the methylation level of the indicated gene in each sample from either primary CRCs of a differing stage or liver metastases. Horizontal lines denote median methylation levels in each group.

observed to be different among the three groups (Table 3). In contrast, DNA methylation–positive cases of *MGMT* were more frequent in stage IV CRCs (40.0%) and in liver metastases (42.4%) than in stage I–III CRCs (20.1%; $P = 0.043$; Table 3). In addition, we found that DNA methylation–positive cases of *TIMP3* were significantly more frequent in liver metastases (15.5%) than in either stage I–III CRCs (3.8%) or stage IV CRCs (0%; $P = 0.028$). These

Table 3. Frequency of DNA Methylation and CIMP Status in Stage I–III CRCs, Stage IV CRCs, and Liver Metastases

	Normal tissue	Stage I–III CRC	Stage IV CRC	Liver metastases	*P* value*
DNA methylation status					
CIMP markers					
P16	0/53 (0)	7/53 (13.2)	3/25 (12.0)	7/62 (11.3)	0.943
hMLH1	0/53 (0)	3/53 (5.6)	2/25 (8.0)	1/62 (1.6)	0.233
MINT1	0/53 (0)	9/53 (17)	4/25 (16.0)	13/62 (21.0)	0.843
MINT2	0/53 (0)	12/53 (22.6)	7/25 (28.0)	6/62 (9.7)	0.060
MINT31	0/53 (0)	30/53 (56.6)	13/25 (52.0)	37/62 (59.7)	0.810
Candidate genes					
MGMT	9/53 (17.0)	11/53 (20.1)	10/25 (40.0)	25/59 (42.4)	0.043
RASSF1A	22/64 (34.4)	21/51 (41.2)	13/23 (56.5)	23/53 (43.4)	0.448
TIMP3	0/8 (0)	2/53 (3.8)	0/23 (0)	9/58 (15.5)	0.028
CDH1	0/8 (0)	0/53 (0)	0/23 (0)	0/59 (0)	NA
Identified genes					
UPK3A	0/8 (0)	0/53 (0)	0/25 (0)	5/59 (8.5)	0.044
CIMP status					
CIMP positive	0/53 (0)	12/53 (22.6)	7/25 (28.0)	15/62 (24.2)	0.871

Data are given as number with methylation/total number, with hypermethylation-positive percentages in parentheses.
NA, not available.
*DNA methylation frequencies were statistically analyzed between stage I–III CRCs, stage IV CRCs, and liver metastases.

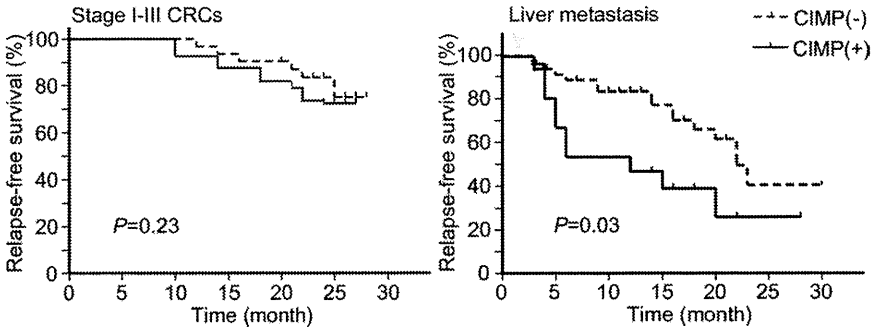

Figure 2. Kaplan-Meier analyses of the probability of RFS in patients with stage I–III CRCs or liver metastases. Both CIMP-negative (n = 31 stage I–III CRCs; n = 47 liver metastases) and CIMP-positive (n = 11 stage I–III CRCs; n = 15 liver metastases) tumors are shown.

data suggest that DNA methylation in a subset of genes progressively increased during the metastatic process in CRC.

Relationship between CIMP Status and Disease Outcome in Stage I–III CRCs and Liver Metastases

Samples with simultaneous methylation of at least two of the five classical CIMP markers were considered CIMP positive.[23] Using this criterion, 12 stage I–III CRCs (22.6%), 7 stage IV CRCs (28.0%), and 15 liver metastases (24.2%) were classified as CIMP positive. There was no difference in relation to the frequency of CIMP-positive cases among the three groups (Table 3).

Several previous studies have demonstrated that CIMP confers variable prognostic effects in CRC.[36–42] We next analyzed the relationship between CIMP status and outcome measurements in patients with stage I–III CRCs and liver metastases (Figure 2). No association was found between CIMP status and RFS in stage I–III CRCs (P = 0.23). In contrast, in the case of liver metastases, CIMP-positive tumors showed significantly earlier recurrence of liver metastasis than did CIMP-negative tumors after treatment (P = 0.030). Incidence of recurrence was marginally associated with the stage of tumors in stage I–III CRCs (P = 0.063) and was significantly associated with CIMP status in liver metastases (P = 0.036), factors that were further analyzed by multivariate analysis. A multivariate analysis using the Cox proportional hazards model showed that clinical stage affected the incidence of recurrence in stage I–III CRCs (hazard ratio = 3.10; 95% confidence interval = 1.04–9.26; P = 0.042; Table 4), whereas CIMP is an independent factor for determining recurrence in liver metastases (hazard ratio = 2.64; 95% confidence interval = 1.18–5.94; P = 0.019; Table 4). These different outcomes of CIMP-positive tumors in stage I–III CRCs and liver metastases raise the possibility that different sets of DNA methylation targets exist in stage I–III CRCs, stage IV CRCs, and liver metastases. To clarify this possibility, we conducted genome-wide DNA methylation analysis in stage I–III CRCs and in paired stage IV primary tumors and liver metastases.

Genome-Wide DNA Methylation Analysis in Stage I–III CRCs and in Paired Stage IV Primary and Liver Metastatic Tumors

To examine genome-wide DNA methylation status according to CRC stage, a microarray-based profiling approach, MCAM, was performed in eight stage I–III CRCs and in nine paired stage IV primary and liver metastatic tumors. The backgrounds of the samples used are shown in Supplemental Table S1 at *http://ajp.amjpathol.org*. Initial validation of the MCAM data showed that a high concordance was observed between the methylation status determined by this technique and pyrosequencing analysis (specificity, 98.8%; sensitivity, 66.7%; and false discovery rate, 0.067; see *Materials and Methods*), as has been demonstrated in previous studies.[26,28,29]

The MCAM analysis revealed that an average of 1213 genes (19.7%), 826 genes (13.4%) and 784 genes (12.7%) were methylated in stage I–III CRCs, stage IV primary CRCs, and liver metastases, respectively (Figure 3A). The number of methylated genes in stage I–III CRCs was significantly larger than that in the other two groups (P = 0.008).

Unsupervised hierarchical clustering analysis of CRCs and liver metastases using the methylation status of 1564 genes, which were methylated in more than two cases of stage I–III CRCs, stage IV primary CRCs, or liver metastases, indicated two major subgroups: one was composed of stage I–III CRCs and another of paired primary and metastatic tumors (Figure 3B). Among the nine paired stage IV tumors, five (cases 3, 5, 6, 7, and 8) showed highly similar methylation profiles (similarity, 85% to 96%), with another (case 4) showing similar methylation profiles (similarity, 65%) between primary tumors and liver metastases (Figure 3B). A distinctly different methylation profile was observed in case 1 between primary tumor and liver metastasis. In this case, the primary tumor was observed to be CIMP positive and the metastatic tumor was less methylated and was deemed to be CIMP negative (see Supplemental Table S1 at *http://ajp.amjpathol.org*). Sampling from different places in the tumor in this case showed consistent results in terms of methylation status (data not shown). Notably, CIMP-positive cases fell into one cluster of each stage (cases 2 and 7 of stage I–III, primary tumors 1 and 3, and liver metastasis 3 of stage IV) (Figure 3B). These data are consistent

Table 4. Analyses of Recurrent Factors for Stage I–III CRC and Liver Metastasis

	Stage I–III CRC (n = 53)		Liver metastasis (n = 62)	
	Value*	P value	Value*	P value
Fisher's Exact Test				
Age, years		0.333		1.000
<60	3/17 (18)		2/6 (33)	
≥60	12/36 (33)		24/56 (43)	
Sex		0.227		0.065
Male	9/24 (38)		17/35 (49)	
Female	6/29 (21)		9/27 (33)	
Stage		0.063		NA
I and II	5/30 (17)		NA	
III	10/23 (43)		NA	
Tumor location		0.736		NA
Proximal	3/13 (23)		NA	
Distal	12/40 (30)		NA	
Metastasis time		NA		0.203
Synchronous	NA		13/37 (35)	
Metachronous	NA		13/25 (52)	
No. of metastatic lesions		NA		0.442
≥3	NA		16/34 (47)	
<3	NA		10/28 (36)	
CIMP		0.722		0.036
Positive	11/41 (27)		16/47 (34)	
Versus negative	4/12 (33)		10/15 (67)	
Multivariate Analysis†				
Age: <60 versus ≥60 years	1.55 (0.39–6.15)	0.532	0.75 (0.17–3.24)	0.702
Sex: male versus female	0.74 (0.24–2.25)	0.594	0.43 (0.18–1.00)	0.051
Stage: III versus I and II	3.10 (1.04–9.26)	0.042	NA	NA
CIMP: positive versus negative	1.05 (0.33–3.39)	0.931	2.64 (1.18–5.94)	0.019

NA, not applicable.
*For Fisher's exact test, values are given as number of recurrences/total number (percentage); for multivariate analysis, values are given as hazard ratio (95% confidence interval).
†Multivariate analysis of recurrent factors by Cox proportional hazards model for stage I–III CRCs and liver metastasis.

with the previous MCAM analysis in CRC, which showed a distinct cluster of CIMP-positive CRCs from other CRC clusters.[29]

To assess whether sets of genes are commonly methylated across multiple cases in primary tumors or liver metastases, silencing of which may foster liver metastasis, we analyzed the methylated genes identified by MCAM analysis. Most of the methylated genes that were commonly methylated across multiple cases (ie, >4 cases) were found to be simultaneously methylated in primary tumors and liver metastases (Figure 3C). In contrast, most of the specific methylation targets in either primary CRCs or liver metastases were found in only one or two cases, suggesting that DNA methylation of a few genes is commonly associated with liver metastasis or that DNA methylation in such specific target genes might be a stochastic event during metastasis (Figure 3C).

Among the specifically hypermethylated genes in liver metastases, as determined by MCAM analysis, we confirmed that *UPK3A* was specifically methylated in these tissues by pyrosequencing analysis, as was found for *TIMP3* (Figure 1, Figure 3D, and Table 3). DNA methylation of this gene was inversely correlated with gene expression levels (Figure 3E). In addition, DNA methylation inhibitor, 5-aza-2′-deoxycytidine, reactivated *UPK3A* gene expression along with DNA demethylation, suggesting that DNA methylation of the *UPK3A* promoter is the primary mechanism underlying silencing of this gene (Figure 3E). Taken together, these data indicate that the methylation profiles of primary and metastatic tumors were similar in most cases and that specific targets of DNA methylation in either primary CRCs or liver metastases might be associated with the metastatic process.

Comparison of Frequently Methylated Genes in Stage I–III CRCs and Stage IV CRCs

Next, we analyzed which genes were frequently methylated in multiple cases of stage I–III CRCs and stage IV CRCs. Unsupervised hierarchical clustering analysis using the methylation status of 630 genes, which were methylated in more than half of the samples in either stage I–III CRCs or stage IV CRCs, showed that stage I–III CRCs and stage IV CRCs were clustered into two subgroups (Figure 4A; see Supplemental Table S2 at *http://ajp.amjpathol.org*). This is consistent with the results of hierarchical clustering analysis using 1564 genes (Figure 3B). Of the 630 genes analyzed, 290 (46.0%) were frequently methylated in stage I–III CRCs and stage IV CRCs, suggesting that hypermethylation of these genes was involved in the transition from early-stage to progressed CRC. In addition, distinct targets were detected in stage I–III CRCs and stage IV CRCs [291 genes (46.2%) in stage I–III CRCs and 49 genes (7.8%) in stage IV CRCs], indicating that frequent methylation targets were different between stage I–III CRCs and stage IV

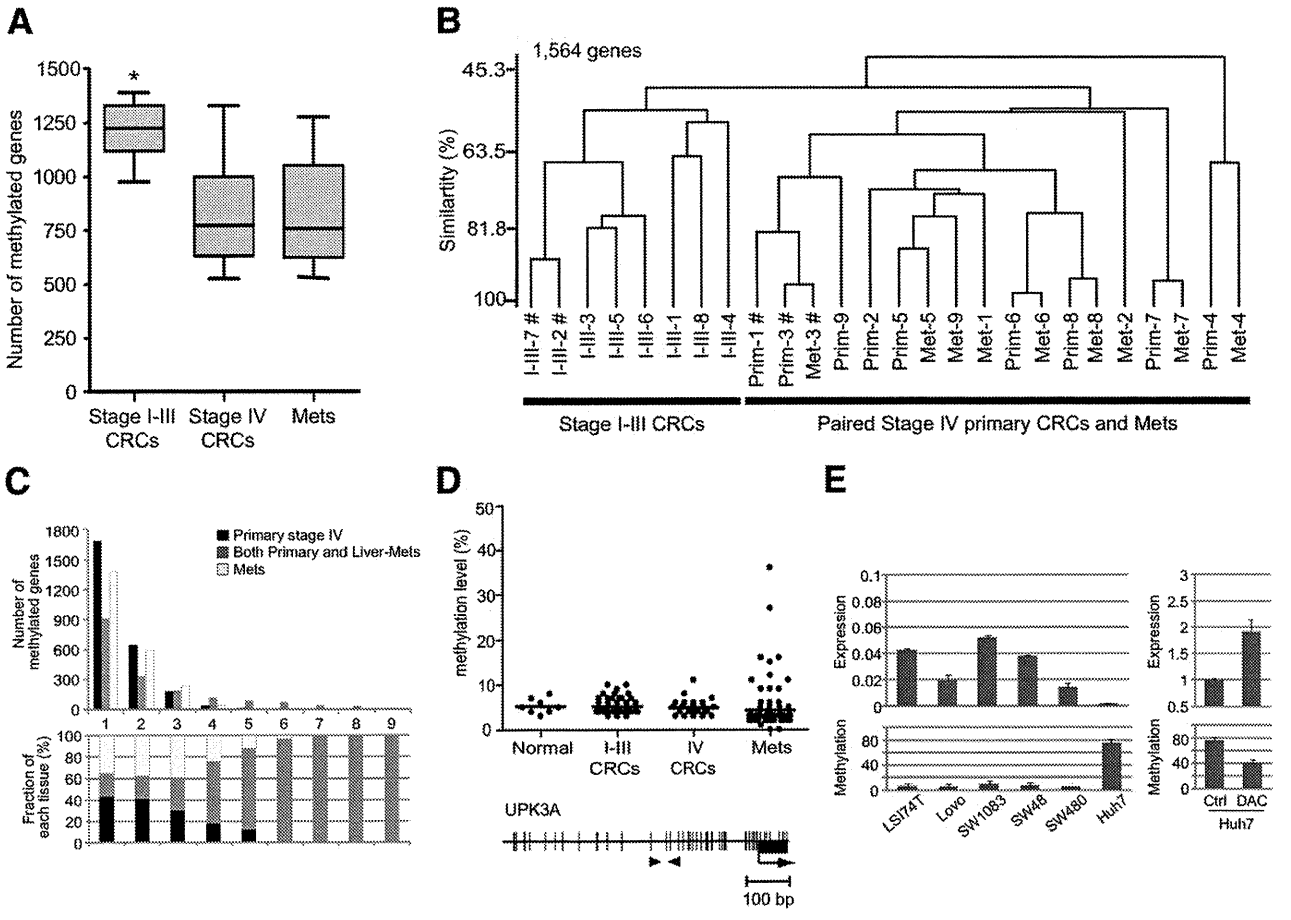

Figure 3. The MCAM analysis in stage I–III CRCs and paired stage IV CRCs and liver metastases. **A:** Box and whisker analysis of the number of methylated genes in stage I–III CRCs and in paired stage IV CRCs and liver metastases (Mets). The median is marked by a bold line inside the box, whose ends denote the upper and lower quartiles. Error bars represent 5 and 95 percentile values. DNA methylation levels were statistically analyzed between stage I–III CRCs, stage IV CRCs, and liver metastases. $^*P = 0.008$. **B:** Dendrogram overview of unsupervised hierarchical cluster analysis using DNA methylation data from 1564 genes assessed via MCAM analysis. I–III, Prim, and Met followed by a number indicate each case of stage I–III CRC, stage IV primary CRC, and liver metastasis, respectively; #, CIMP-positive tumor. **C:** Number of genes (*y* axis) that were commonly methylated in x number of cases, where x is the axis in stage IV primary tumor (black), liver metastasis (white), or both primary and liver metastasis (gray) (**top**), and the fraction of each tissue that has commonly methylated genes in x number of cases (**bottom**). **D:** DNA methylation status of the *UPK3A* gene in 53 stage I–III CRCs, 25 stage IV CRCs, and 62 liver metastases (**top**) and a schematic diagram of the promoter of the *UPK3A* gene (**bottom**). The transcription start site (**arrow**) and the location of exon 1 (**black box**) are indicated. **Black arrowheads** indicate the regions analyzed by pyrosequencing. Scatterplot represents the same as in Figure 1. **E:** Gene expression (**top left**) and DNA methylation (**bottom left**) of *UPK3A* were measured by quantitative PCR and pyrosequencing analysis in six cell lines, respectively. After treatment with 5-aza-2′-deoxycytidine (1 μmol/L), *UPK3A* was reactivated (**top right**) with a decreased level of DNA methylation (**top right**). Ctrl, cells treated with distilled water. Relative values of mRNA expression for the *UPK3A* gene to glyceraldehyde-3-phosphate dehydrogenase are shown on the *y* axis (**top**). Error bars denote SDs from experiments in triplicate.

CRCs, which may be associated with the different pathologic features of the two groups.

Based on the results of the MCAM assay, along with annotation analysis and characterization of target genes, two representative genes, *ANK1* and *CYBRD1*, which have a typical CpG island containing two XmaI recognition sites closely located at the transcription start site of the genes, were selected and further examined by pyrosequencing analysis. Because CpG contents around the transcription start sites of the *ANK1* and *CYBRD1* genes are extensively high, we designed primers downstream of exon 1 for both genes (Figure 4B). We further designed MSP assays encompassing the transcription start sites and found that methylation status determined using the pyrosequencing and MSP assays were concordant (see Supplemental Figure S1 at *http://ajp.amjpathol.org*). Consistent with the MCAM data, pyrosequencing analysis revealed that *ANK1* showed a higher level of DNA methylation in stage IV CRCs than in stage I–III CRCs ($P = 0.002$; Figure 4C), whereas *CYBRD1* showed a higher DNA methylation level in stage I–III CRCs than in stage IV CRCs ($P = 0.048$; Figure 4C).

Discussion

Cancer metastasis is a complex process involving many biological steps, presumably requiring significant changes in gene expression.[9] Several studies have suggested a contribution of epigenetic abnormalities during the process of CRC metastasis[19,38,43]; however, genome-wide epigenetic alterations have not so far been studied in this context. In this study, we comprehensively examined methylation status in primary CRCs and liver

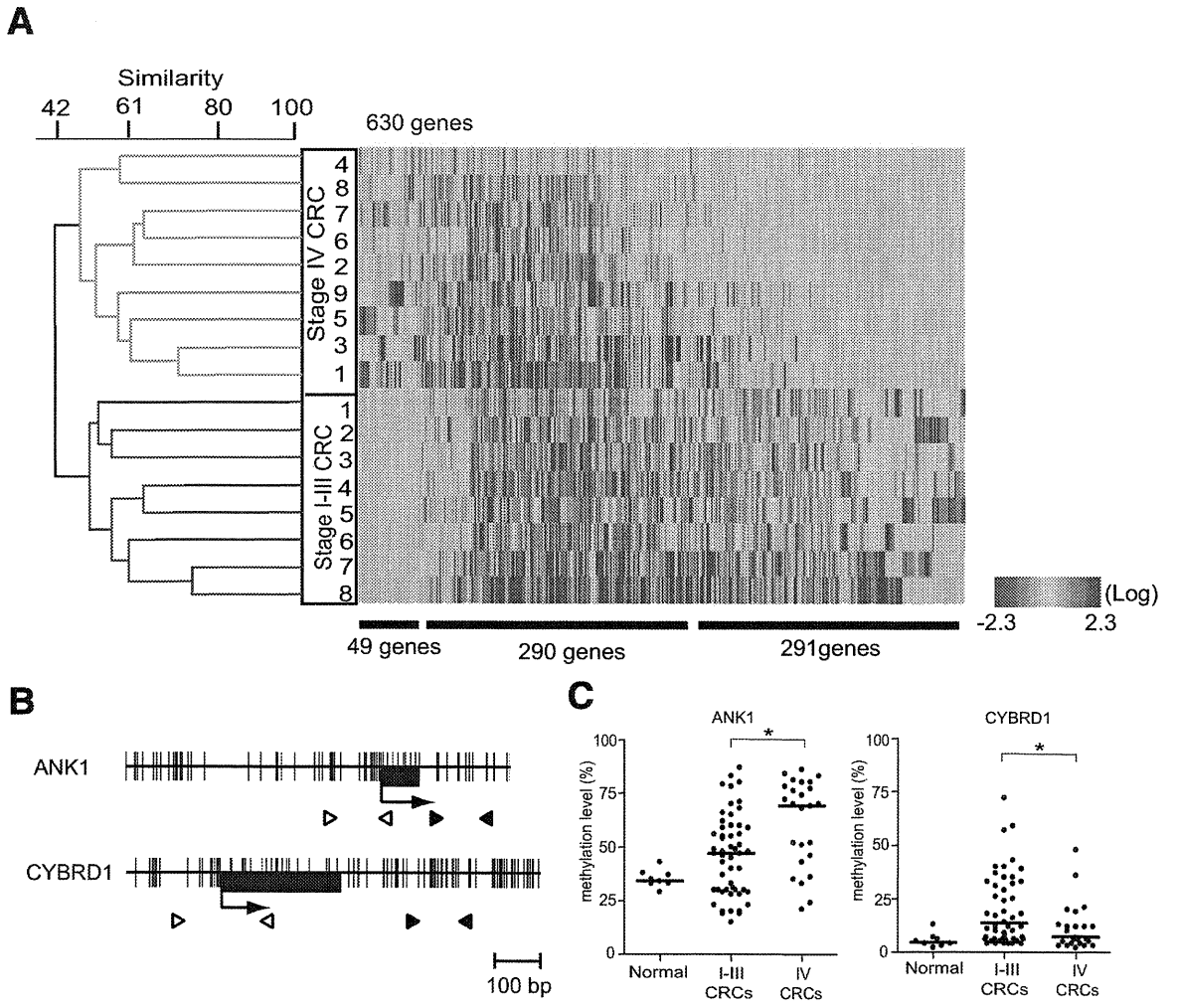

Figure 4. Dendrogram and heat map overview of unsupervised hierarchical cluster analysis of DNA methylation data from stage I–III CRCs and stage IV CRCs using 630 genes. **A:** Commonly methylated genes in either stage I–III CRCs or stage IV CRCs are analyzed. Each cell in the matrix represents the DNA methylation status of a gene in an individual sample. Red and blue in cells reflect high and low methylation levels, respectively, as indicated in the scale bar (log2-transformed scale). Numbers below the matrix indicate the methylated genes frequently found in stage IV CRCs, in both stage I–III CRCs and stage IV CRCs, and in stage I–III CRCs, respectively. The dendrogram represents the same as Figure 3. **B:** Schematic diagrams of the promoters of the *ANK1* and *CYBRD1* genes. The transcription start site (**arrow**) and the location of exon 1 (**black box**) are indicated. **Black** and **white arrowheads** indicate the regions analyzed by pyrosequencing and MSP, respectively. **C:** DNA methylation status of the *ANK1* and *CYBRD1* genes in 8 normal tissues, 53 stage I–III CRCs, and 25 stage IV CRCs. Scatterplot represents the same as Figure 1. DNA methylation levels were statistically analyzed between stage I–III CRCs and stage IV CRCs. $^{*}P < 0.05$.

metastases to decipher the contribution of aberrant DNA methylation to liver metastasis. Frequencies of DNA methylation in the present study, which were assessed by pyrosequencing analysis, were a little lower than were those in the previous studies using MSP or combined bisulfite restriction analysis.[32,35,44,45] The differences in the methylation status might be due to the different technology used for methylation analysis.

Methylation frequencies of *MGMT* and *TIMP3* were progressively increased during the metastatic process in CRC. *MGMT* is a DNA repair gene that is frequently methylated in CRC and is correlated with G to A transition mutations in cancer-related genes, such as *KRAS, TP53,* and *PIK3CA*.[46–49] *MGMT* hypermethylation has been reported to occur during the very early steps of colorectal carcinogenesis.[32] In this study, we showed that the methylation frequency of *MGMT* is significantly increased from stage I–III CRC to stage IV CRC and liver metastasis, suggesting that hypermethylation of *MGMT* may also contribute to disease progression. *TIMP3* is a natural inhibitor for matrix metalloproteinase and is involved in the degradation of extracellular matrix.[50] Attenuated expression of *TIMP3* protein is related to the infiltration and metastasis of CRC.[51] The present data are consistent with a major role for *TIMP3* in CRC metastasis, supporting the idea that silencing of *TIMP3* in tumor cells might confer potency for metastasis to other organs. In addition to these two genes, we newly identified *UPK3A* as being methylated only in liver metastases in the present study. *UPK3A* encodes for a member of the uroplakin family, a group of transmembrane proteins that form complexes on the apical surface of the bladder epithelium.[52] Loss of expression of uroplakin 3 is associated with aggressive bladder cancer.[53] These data indicate that silencing of *UPK3A* by DNA methylation may contribute to the establishment of liver metastasis during the progression of

CRC. In addition, our results have profound implications for screening and diagnosis of liver metastasis in CRC. The aberrant DNA methylation of *TIMP3*, *MGMT,* and *UPK3A* could serve as informative markers of liver metastasis and could be applicable to the samples obtained from less invasive procedures, such as serum.[54] A larger study is needed to validate these three genes as useful diagnostic markers for liver metastasis.

Several studies have demonstrated variable prognostic effects with respect to the impact of DNA methylation in CRC.[36–41,55–58] Studies showed CIMP as a predictor of better prognosis in CRCs.[37,56] Another study examined CIMP in stage IV CRCs treated with 5-fluorouracil–based chemotherapy and found that CIMP predicts poor prognosis.[58] Recent studies showed that worse outcome of CIMP-positive tumors is driven by *BRAF* mutation.[37,38,40] However, despite the numerous studies in CRCs, the relative contributions of these parameters to survival outcome need to be further investigated to understand the effects and interactions of these variables.[59]

In this study, there was no difference in CIMP frequency among stage I–III CRCs, stage IV CRCs, and liver metastases, suggesting that CIMP is not a predictor of liver metastasis. However, in relation to the prognostic potential of CIMP status, CIMP-positive cases showed significantly earlier recurrence than did CIMP-negative cases when liver metastases were assessed, whereas there was no difference in RFS between CIMP-positive and CIMP-negative stage I–III CRCs. In the present cohort, we found on a preliminary basis that frequencies of *BRAF* mutation at codon 600, which was assessed by pyrosequencing analysis,[29] are 3 of 77 (4%) and 1 of 54 (2%) in stage I–IV CRCs and liver metastases, respectively. This low incidence of *BRAF* mutation in this cohort did not affect the analysis for RFS (data not shown). One plausible explanation for the inconsistent links to outcome regarding CIMP status between different stages in the present study may due to an existence of certain sets of hypermethylated genes between stage I–III CRCs and stage IV CRCs. Indeed, the global MCAM analysis revealed distinctly altered methylation profiles between stage I–III CRCs and stage IV CRCs. The number of methylation targets in stage IV CRCs is smaller than that observed in stage I–III CRCs. Given the paradigm concept of progression to metastasis occurring through stepwise genetic and epigenetic evolution, this result is somewhat unexpected. A conceivable hypothesis is that tumors with high degrees of methylation are more likely to inactivate genes critical for tumor progression and metastasis.

More than 60% of cases showed similar methylation profiles between paired stage IV primary tumors and liver metastases. Although we found a few genes differentially methylated between primary stage IV tumors and liver metastases, in which aberrant methylation might occur after metastasis during expansion of the clone in the liver, these data suggest that most methylation changes in these tumors may be established before progression to liver metastasis.

Recent experimental and conceptual models are beginning to address the genetic basis for cancer metastasis.[16] Cancer metastasis has been explained by at least two models, namely, a progression model and an initiating model.[60–62] In the progression model, metastatic capacity is acquired during cancer progression in a subpopulation of cells through sequential genetic mutations or epigenetic alterations, whereas in the initiation model, cells with metastatic potential are determined by early mutational events.[6,16] Because DNA methylation is generally inherited stably, methylation profiles may reflect a signature of tumor evolution. Distinct methylation profiles in stage I–III CRCs and stage IV CRCs are partially explained by the initiating model, where metastatic potential is determined by characteristic epigenetic events in each tumor cell.[16,62] In the paired primary CRCs and liver metastases, one case was CIMP positive based on analysis of the primary lesion but CIMP negative when the metastatic lesion was assessed. This also seems to be consistent with the initiation model in which progenitor cells with different CIMP statuses coexist in a tumor and may develop independently. In this case, cells with metastatic potential are CIMP negative and a minor population in a primary tumor. Taken together, the global epigenetic analysis supports the initiating model in many CRCs. Although the underlying biological complexity of cancer suggests that both initiating and progression models probably contribute to liver metastasis, cancer metastasis potential is not necessarily acquired during progression.

In conclusion, we demonstrated significant implications for epigenetic alterations in stage I–III CRCs, stage IV CRCs, and liver metastases using genome-wide methylation profiling and comprehensive quantitative methylation analysis. Although the genome-wide DNA methylation analyses were performed in a discrete cohort, we showed that DNA methylation profiles may evolve differently in stage I–III CRCs and stage IV CRCs, which likely reflects different pathologic processes. Larger studies might be desired to clarify that stage IV CRCs and stage I–III CRCs have a fundamental difference in terms of epigenetic evolution. These results have strong implications for early detection, screening, and diagnosis of highly metastatic CRCs using differentially methylated genes between stage I–III CRCs and stage IV CRCs.

Acknowledgments

We thank Ikuko Tomimatsu for her technical assistance and Shana Straub for her critical reading of the manuscript.

References

1. Jemal A, Siegel R, Ward E, Hao Y, Xu J, Murray T, Thun MJ: Cancer statistics, 2008. CA Cancer J Clin 2008, 58:71–96
2. Scheele J, Stang R, Altendorf-Hofmann A, Paul M: Resection of colorectal liver metastases. World J Surg 1995, 19:59–71
3. Mayo SC, Pawlik TM: Current management of colorectal hepatic metastasis. Expert Rev Gastroenterol Hepatol 2009, 3:131–144
4. Taylor M, Forster J, Langer B, Taylor BR, Greig PD, Mahut C: A study of prognostic factors for hepatic resection for colorectal metastases. Am J Surg 1997, 173:467–471

5. Nikfarjam M, Shereef S, Kimchi ET, Gusani NJ, Jiang Y, Avella DM, Mahraj RP, Staveley-O'Carroll KF: Survival outcomes of patients with colorectal liver metastases following hepatic resection or ablation in the era of effective chemotherapy. Ann Surg Oncol 2009, 16:1860–1867
6. Gray JW: Evidence emerges for early metastasis and parallel evolution of primary and metastatic tumors. Cancer Cell 2003, 4:4–6
7. Nguyen DX, Bos PD, Massague J: Metastasis: from dissemination to organ-specific colonization. Nat Rev Cancer 2009, 9:274–284
8. Gray J: Cancer: genomics of metastasis. Nature 2010, 464:989–990
9. Hynes RO: Metastatic potential: generic predisposition of the primary tumor or rare, metastatic variants-or both? Cell 2003, 113:821–823
10. Bird NC, Mangnall D, Majeed AW: Biology of colorectal liver metastases: a review. J Surg Oncol 2006, 94:68–80
11. Nagashima Y, Hasegawa S, Koshikawa N, Taki A, Ichikawa Y, Kitamura H, Misugi K, Kihira Y, Matuo Y, Yasumitsu H, Miyazaki K: Expression of matrilysin in vascular endothelial cells adjacent to matrilysin-producing tumors. Int J Cancer 1997, 72:441–445
12. Furger KA, Menon RK, Tuck AB, Bramwell VH, Chambers AF: The functional and clinical roles of osteopontin in cancer and metastasis. Curr Mol Med 2001, 1:621–632
13. Weber GF: Molecular mechanisms of metastasis. Cancer Lett 2008, 270:181–190
14. Folkman J: What is the evidence that tumors are angiogenesis dependent? J Natl Cancer Inst 1990, 82:4–6
15. Kioi M, Yamamoto K, Higashi S, Koshikawa N, Fujita K, Miyazaki K: Matrilysin (MMP-7) induces homotypic adhesion of human colon cancer cells and enhances their metastatic potential in nude mouse model. Oncogene 2003, 22:8662–8670
16. Threadgill DW: Metastatic potential as a heritable trait. Nat Genet 2005, 37:1026–1027
17. Jones PA, Takai D: The role of DNA methylation in mammalian epigenetics. Science 2001, 293:1068–1070
18. Herman JG, Baylin SB: Gene silencing in cancer in association with promoter hypermethylation. N Engl J Med 2003, 349:2042–2054
19. Miranda E, Destro A, Malesci A, Balladore E, Bianchi P, Baryshnikova E, Franchi G, Morenghi E, Laghi L, Gennari L, Roncalli M: Genetic and epigenetic changes in primary metastatic and nonmetastatic colorectal cancer. Br J Cancer 2006, 95:1101–1107
20. Lui EL, Loo WT, Zhu L, Cheung MN, Chow LW: DNA hypermethylation of TIMP3 gene in invasive breast ductal carcinoma. Biomed Pharmacother 2005, 59(Suppl 2):S363–S365
21. Fendri A, Masmoudi A, Khabir A, Sellami-Boudawara T, Daoud J, Frikha M, Ghorbel A, Gargouri A, Mokdad-Gargouri R: Inactivation of RASSF1A, RARbeta2 and DAP-kinase by promoter methylation correlates with lymph node metastasis in nasopharyngeal carcinoma. Cancer Biol Ther 2009, 8:444–451
22. Toyota M, Ahuja N, Ohe-Toyota M, Herman JG, Baylin SB, Issa JP: CpG island methylator phenotype in colorectal cancer, Proc Natl Acad Sci U S A 1999, 96:8681–8686
23. Issa JP: CpG island methylator phenotype in cancer. Nat Rev Cancer 2004, 4:988–993
24. Boland CR, Goel A: Somatic evolution of cancer cells. Semin Cancer Biol 2005, 15:436–450
25. Shen L, Kondo Y, Guo Y, Zhang J, Zhang L, Ahmed S, Shu J, Chen X, Waterland RA, Issa JP: Genome-wide profiling of DNA methylation reveals a class of normally methylated CpG island promoters. PLoS Genet 2007, 3:2023–2036
26. Gao W, Kondo Y, Shen L, Shimizu Y, Sano T, Yamao K, Natsume A, Goto Y, Ito M, Murakami H, Osada H, Zhang J, Issa JP, Sekido Y: Variable DNA methylation patterns associated with progression of disease in hepatocellular carcinomas. Carcinogenesis 2008, 29:1901–1910
27. Omura N, Li CP, Li A, Hong SM, Walter K, Jimeno A, Hidalgo M, Goggins M: Genome-wide profiling of methylated promoters in pancreatic adenocarcinoma. Cancer Biol Ther 2008, 7:1146–1156
28. Goto Y, Shinjo K, Kondo Y, Shen L, Toyota M, Suzuki H, Gao W, An B, Fujii M, Murakami H, Osada H, Taniguchi T, Usami N, Kondo M, Hasegawa Y, Shimokata K, Matsuo K, Hida T, Fujimoto N, Kishimoto T, Issa JP, Sekido Y: Epigenetic profiles distinguish malignant pleural mesothelioma from lung adenocarcinoma. Cancer Res 2009, 69:9073–9082
29. An B, Kondo Y, Okamoto Y, Shinjo K, Kanemitsu Y, Komori K, Hirai T, Sawaki A, Tajika M, Nakamura T, Yamao K, Yatabe Y, Fujii M, Murakami H, Osada H, Tani T, Matsuo K, Shen L, Issa JP, Sekido Y: A characteristic methylation profile in CpG island methylator phenotype-negative distal colorectal cancers. Int J Cancer 2010, 127:2095–2105
30. Greene FL, Sobin LH: The TNM system: our language for cancer care. J Surg Oncol 2002, 80:119–120
31. Mori D, Shibaki M, Masuda M, Yamasaki F: Quantitative measurement of venous invasion of colorectal cancer with metachronous liver metastasis. Histopathology 2009, 55:654–659
32. Shen L, Kondo Y, Rosner GL, Xiao L, Hernandez NS, Vilaythong J, Houlihan PS, Krouse RS, Prasad AR, Einspahr JG, Buckmeier J, Alberts DS, Hamilton SR, Issa JP: MGMT promoter methylation and field defect in sporadic colorectal cancer. J Natl Cancer Inst 2005, 97:1330–1338
33. Eisen MB, Spellman PT, Brown PO, Botstein D: Cluster analysis and display of genome-wide expression patterns. Proc Natl Acad Sci U S A 1998, 95:14863–14868
34. Liu L, Broaddus RR, Yao JC, Xie S, White JA, Wu TT, Hamilton SR, Rashid A: Epigenetic alterations in neuroendocrine tumors: methylation of RAS-association domain family 1, isoform A and p16 genes are associated with metastasis. Mod Pathol 2005, 18:1632–1640
35. Kim YH, Petko Z, Dzieciatkowski S, Lin L, Ghiassi M, Stain S, Chapman WC, Washington MK, Willis J, Markowitz SD, Grady WM: CpG island methylation of genes accumulates during the adenoma progression step of the multistep pathogenesis of colorectal cancer. Genes Chromosomes Cancer 2006, 45:781–789
36. Barault L, Charon-Barra C, Jooste V, de la Vega MF, Martin L, Roignot P, Rat P, Bouvier AM, Laurent-Puig P, Faivre J, Chapusot C, Piard F: Hypermethylator phenotype in sporadic colon cancer: study on a population-based series of 582 cases. Cancer Res 2008, 68:8541–8546
37. Ogino S, Nosho K, Kirkner GJ, Kawasaki T, Meyerhardt JA, Loda M, Giovannucci EL, Fuchs CS: CpG island methylator phenotype, microsatellite instability: BRAF mutation and clinical outcome in colon cancer. Gut 2009, 58:90–96
38. Kim JH, Shin SH, Kwon HJ, Cho NY, Kang GH: Prognostic implications of CpG island hypermethylator phenotype in colorectal cancers. Virchows Arch 2009, 455:485–494
39. Samowitz WS, Sweeney C, Herrick J, Albertsen H, Levin TR, Murtaugh MA, Wolff RK, Slattery ML: Poor survival associated with the BRAF V600E mutation in microsatellite-stable colon cancers. Cancer Res 2005, 65:6063–6069
40. Dahlin AM, Palmqvist R, Henriksson ML, Jacobsson M, Eklof V, Rutegard J, Oberg A, Van Guelpen BR: The role of the CpG island methylator phenotype in colorectal cancer prognosis depends on microsatellite instability screening status. Clin Cancer Res 2010, 16:1845–1855
41. Sanchez JA, Krumroy L, Plummer S, Aung P, Merkulova A, Skacel M, DeJulius KL, Manilich E, Church JM, Casey G, Kalady MF: Genetic and epigenetic classifications define clinical phenotypes and determine patient outcomes in colorectal cancer. Br J Surg 2009, 96:1196–1204
42. Yagi K, Akagi K, Hayashi H, Nagae G, Tsuji S, Isagawa T, Midorikawa Y, Nishimura Y, Sakamoto H, Seto Y, Aburatani H, Kaneda A: Three DNA methylation epigenotypes in human colorectal cancer. Clin Cancer Res 2010, 16:21–33
43. Chen J, Rocken C, Lofton-Day C, Schulz HU, Muller O, Kutzner N, Malfertheiner P, Ebert MP: Molecular analysis of APC promoter methylation and protein expression in colorectal cancer metastasis. Carcinogenesis 2005, 26:37–43
44. Ogino S, Cantor M, Kawasaki T, Brahmandam M, Kirkner GJ, Weisenberger DJ, Campan M, Laird PW, Loda M, Fuchs CS: CpG island methylator phenotype (CIMP) of colorectal cancer is best characterised by quantitative DNA methylation analysis and prospective cohort studies. Gut 2006, 55:1000–1006
45. Shen L, Toyota M, Kondo Y, Lin E, Zhang L, Guo Y, Hernandez NS, Chen X, Ahmed S, Konishi K, Hamilton SR, Issa JP: Integrated genetic and epigenetic analysis identifies three different subclasses of colon cancer. Proc Natl Acad Sci U S A 2007, 104:18654–18659
46. Esteller M, Toyota M, Sanchez-Cespedes M, Capella G, Peinado MA, Watkins DN, Issa JP, Sidransky D, Baylin SB, Herman JG: Inactivation of the DNA repair gene O6-methylguanine-DNA methyltransferase by promoter hypermethylation is associated with G to A mutations in K-ras in colorectal tumorigenesis. Cancer Res 2000, 60:2368–2371
47. Esteller M, Risques RA, Toyota M, Capella G, Moreno V, Peinado MA, Baylin SB, Herman JG: Promoter hypermethylation of the DNA repair gene O(6)-methylguanine-DNA methyltransferase is associated with

the presence of G: C to A:T transition mutations in p53 in human colorectal tumorigenesis. Cancer Res 2001, 61:4689–4692
48. Halford S, Rowan A, Sawyer E, Talbot I, Tomlinson I: O(6)-methylguanine methyltransferase in colorectal cancers: detection of mutations, loss of expression, and weak association with G:C>A:T transitions. Gut 2005, 54:797–802
49. Nosho K, Kawasaki T, Ohnishi M, Suemoto Y, Kirkner GJ, Zepf D, Yan L, Longtine JA, Fuchs CS, Ogino S: PIK3CA mutation in colorectal cancer: relationship with genetic and epigenetic alterations. Neoplasia 2008, 10:534–541
50. Chambers AF, Matrisian LM: Changing views of the role of matrix metalloproteinases in metastasis. J Natl Cancer Inst 1997, 89:1260–1270
51. Bai YX, Yi JL, Li JF, Sui H: Clinicopathologic significance of BAG1 and TIMP3 expression in colon carcinoma. World J Gastroenterol 2007, 13:3883–3885
52. Wu XR, Lin JH, Walz T, Haner M, Yu J, Aebi U, Sun TT: Mammalian uroplakins: a group of highly conserved urothelial differentiation-related membrane proteins. J Biol Chem 1994, 269:13716–13724
53. Matsumoto K, Satoh T, Irie A, Ishii J, Kuwao S, Iwamura M, Baba S: Loss expression of uroplakin III is associated with clinicopathologic features of aggressive bladder cancer. Urology 2008, 72:444–449
54. Nakayama H, Hibi K, Taguchi M, Takase T, Yamazaki T, Kasai Y, Ito K, Akiyama S, Nakao A: Molecular detection of p16 promoter methylation in the serum of colorectal cancer patients. Cancer Lett 2002, 188:115–119
55. Esteller M, Gonzalez S, Risques RA, Marcuello E, Mangues R, Germa JR, Herman JG, Capella G, Peinado MA: K-ras and p16 aberrations confer poor prognosis in human colorectal cancer. J Clin Oncol 2001, 19:299–304
56. Van Rijnsoever M, Elsaleh H, Joseph D, McCaul K, Iacopetta B: CpG island methylator phenotype is an independent predictor of survival benefit from 5-fluorouracil in stage III colorectal cancer. Clin Cancer Res 2003, 9:2898–2903
57. Ward RL, Cheong K, Ku SL, Meagher A, O'Connor T, Hawkins NJ: Adverse prognostic effect of methylation in colorectal cancer is reversed by microsatellite instability. J Clin Oncol 2003, 21:3729–3736
58. Shen L, Catalano PJ, Benson AB III, O'Dwyer P, Hamilton SR, Issa JP: Association between DNA methylation and shortened survival in patients with advanced colorectal cancer treated with 5-fluorouracil based chemotherapy. Clin Cancer Res 2007, 13:6093–6098
59. Walther A, Johnstone E, Swanton C, Midgley R, Tomlinson I, Kerr D: Genetic prognostic and predictive markers in colorectal cancer. Nat Rev Cancer 2009, 9:489–499
60. Nowell PC: The clonal evolution of tumor cell populations. Science 1976, 194:23–28
61. Fidler IJ, Kripke ML: Metastasis results from preexisting variant cells within a malignant tumor. Science 1977, 197:893–895
62. Ramaswamy S, Ross KN, Lander ES, Golub TR: A molecular signature of metastasis in primary solid tumors. Nat Genet 2003, 33:49–54

European Journal of Pharmacology 651 (2011) 18–25

Contents lists available at ScienceDirect

European Journal of Pharmacology

journal homepage: www.elsevier.com/locate/ejphar

Molecular and Cellular Pharmacology

Inhibition of cell survival, invasion, tumor growth and histone deacetylase activity by the dietary flavonoid luteolin in human epithelioid cancer cells

Samir Attoub [a,f,*], Ahmed H. Hassan [b], Barbara Vanhoecke [c], Rabah Iratni [d], Takashi Takahashi [e], Anne-Marie Gaben [f], Marc Bracke [c], Salma Awad [b], Anne John [a], Hamda Ahmed Kamalboor [a], Mahmood Ahmed Al Sultan [a], Kholoud Arafat [a], Christian Gespach [f], Georg Petroianu [a]

[a] Department of Pharmacology & Therapeutics, Faculty of Medicine & Health Sciences, United Arab Emirates University, Al-Ain, P.O. Box: 17666, United Arab Emirates
[b] Department of Biochemistry, Faculty of Medicine & Health Sciences, United Arab Emirates University, Al-Ain, P.O. Box: 17666, United Arab Emirates
[c] Laboratory of Experimental Cancer Research, University Hospital, De Pintelaan 185, B-9000 Gent, Belgium
[d] Department of Biology, United Arab Emirates University, P. O. Box: 17551, Al Ain, United Arab Emirates
[e] Division of Molecular Carcinogenesis, Center for Neurological Diseases and Cancer, Nagoya University Graduate School of Medicine 65 Tsurumai-cho, Showa-ku, Nagoya 466-8550, Japan
[f] INSERM U673 and U938, University Pierre et Marie Curie, Paris VI, Hospital Saint-Antoine, 75571 Paris Cedex 12, France

ARTICLE INFO

Article history:
Received 26 June 2010
Received in revised form 14 October 2010
Accepted 31 October 2010
Available online 11 November 2010

Keywords:
Lung and breast cancer
Luteolin
Viability
Invasion
Caspase-3
Histones H3/H4

ABSTRACT

Phytochemical compounds and histone deacetylase (HDAC) inhibitors are emerging as a new generation of anticancer agents with limited toxicity in cancer patients. We investigated the impact of luteolin, a dietary flavonoid, on survival, migration, invasion of cancer cells *in vitro*, and tumor growth *in vivo*. Luteolin (25–200 μM) decreased the viability of human cancer cell lines originating from the lung (LNM35), colon (HT29), liver (HepG2) and breast (MCF7/6 and MDA-MB231-1833). Luteolin effectively increased the sub-G1 (apoptotic) fraction of cells through caspase-3 and -7 dependent pathways. We provide evidence that luteolin at sub-lethal/non-toxic concentrations inhibited the invasive potential of LNM35, MCF-7/6 and MDA-MB231-1833 cancer cells using Matrigel as well as the chick heart and Oris invasion assays. Moreover, we demonstrate for the first time that luteolin is a potent HDAC inhibitor that potentiates the cytotoxicity of cisplatin in LNM35 cells and decreases the growth of LNM35 tumor xenografts in athymic mice after intraperitoneal injection (20 mg/kg/day for 18 days) Thus, luteolin, in combination with standard anticancer drugs such as cisplatin, may be a promising HDAC inhibitor for the treatment of lung cancer.

1. Introduction

Cancer is a leading cause of death worldwide with about 20,000 global cancer deaths per day in 2007. Lung cancer is the most common form of cancer with the highest mortality rates in the world and breast cancer is the most common cancer seen in women accounting for more than 1.5 million new cases diagnosed in 2010 and an estimated 1 million deaths each year worldwide (Parkin et al., 2005).

Despite advances in the molecular biology of cancer, improved diagnosis and new targeted therapies, cures for most types of cancer remain elusive. To improve cancer patient survival, we need to develop new cytotoxic compounds with selective molecular targeting. Herbal treatments are used in cancer therapy, and several plant-derived compounds have been successfully tried in the clinic. These include vinca alcaloids such as vinblastine (Velban), vincristine (Oncovin), and vinorelbine (Navelbine); topoisomerase I and II inhibitors topotecan (Hycamtin), irinotecan (Camptosar), etoposide (VP-16; VePesid), teniposide (VM-26; Vumon); and taxanes paclitaxel (Taxol), docetaxel (Taxotere) (Coseri, 2009).

Over the last years, there is growing interest in phytochemical compounds with anticancer potential and low toxicity. Flavonoids belong to a vast group of polyphenolic compounds that are widely distributed in plant-derived foods. They contribute to the flavour and colour of fruits and vegetables. The six major sub-classes of flavonoids comprise flavones (e.g., apigenin and luteolin), flavonols (e.g., quercetin and myricetin), flavanones (e.g., naringenin and hesperidin), catechins or flavanols (e.g., epicatechin and gallocatechin), anthocyanidins (e.g., cyanidin and pelargonidin), and isoflavones (e.g., genistein and daidzein).

Interest in the potential health benefits of flavonoids has increased owing to their potent antioxidant and free-radical scavenging activities observed *in vitro*. However, epidemiological studies exploring the role of flavonoids in human health have been inconclusive, and so further studies are warranted (Ross and Kasum, 2002; Strick et al., 2000).

Luteolin, 3′,4′,5,7-tetrahydroxyflavone, is a common flavonoid found in fruits, vegetables, and medicinal herbs. Plants rich in luteolin have been used in Chinese traditional medicine for treating various

* Corresponding author. Department of Pharmacology, Faculty of Medicine and Health Sciences, United Arabs Emirates University, P.O. Box 17666, Al Ain, United Arab Emirates. Tel.: +971 3 7137 219; fax: +971 3 767 2033.
E-mail address: samir.attoub@uaeu.ac.ae (S. Attoub).

0014-2999/$ – see front matter © 2010 Elsevier B.V. All rights reserved.
doi:10.1016/j.ejphar.2010.10.063

diseases such as hypertension, inflammatory disorders, and cancer. In the present study, we investigated the effect of luteolin on human lung, colon, liver and breast cancer cell survival and apoptosis, migration, invasion, tumor growth, and acetylation levels of histones H3 and H4.

2. Materials and methods

2.1. Cell culture and reagents

Human lung cancer cells LNM35 (NSCLC) (Kozaki et al., 2000) were maintained in RPMI 1640 (Invitrogen, Cergy Pontoise, France), human colorectal cancer cells HT29, human hepatoma cells HepG2 and breast MDA-MB-213-1833 cells were maintained in DMEM (Invitrogen, Cergy Pontoise, France). Human breast cancer cells MCF-7/6 were maintained in 50:50 DMEM/HAMF12 media (Invitrogen, Merelbeke, Belgium). All media were supplemented with 10% fetal bovine serum (Roche Molecular Biochemicals, Meylan, France). Luteolin was purchased from Sigma-Aldrich (Saint-Quentin Fallavier, France).

2.2. Cellular viability

Cells were seeded at a density of 5000 cells/well into 96-well plates. After 24 h, cells were treated for 24 h with increasing concentrations of luteolin (1–200 μM), in triplicate. Control cultures were treated with 0.1% DMSO. The effect of luteolin on cell viability was determined using a CellTiter-Glo Luminescent Cell Viability assay (Promega Corporation, Madison), based on quantification of ATP, which signals the presence of metabolically active cells. The luminescent signal was measured using the GLOMAX Luminometer system. Data were presented as proportional viability (%) by comparing the treated group with the untreated cells, the viability of which is assumed to be 100%.

2.3. Detection of sub-G1 cells

LNM35 cells (1×10^6) were plated and cultured at 37 °C on 100-mm Petri dishes in RPMI supplemented with 10% FBS. After 24 h, cells were treated with 50 μM luteolin or 0.1% DMSO for 24 h in RPMI 10% FBS. For flow cytometric analysis, adherent and floating cells were combined, washed once with PBS, and fixed overnight at 4 °C in 70% ethanol. Subsequently cells were washed with PBS, incubated for 30 min at 37 °C with 1 μg/ml RNase A, stained with propidium iodide and analyzed for relative DNA content using a FACScan flow cytometer (FACSCalibur; Becton Dickinson, Le Pont de Claix, France). About 10,000 cells were recorded per assay.

2.4. Caspase 3/7 activity

LNM35 cells were seeded at the density of 5000 cells/well into 96-well plate and treated with 50 μM luteolin for 24 h, in triplicate. Caspase-3/7 activity was measured using a luminescent Caspase-Glo 3/7 assay kit following the manufacturer's instructions (Promega Corporation, Madison, USA). Caspase reagent was added and the plate was mixed using an orbital shaker and incubated for 2.5 h at room temperature. Luminescence was measured using a GLOMAX Luminometer system.

2.5. HDAC assay and histone acetylation levels

To determine the HDAC inhibitory activity of luteolin, we used a colorimetric HDAC Activity Assay Kit (Millipore/Upstate, USA) and followed the manufacturer's instructions with some modifications. Acetyl-conjugated histone H3 and H4 peptides (the substrate) were incubated with HeLa nuclear extract (rich in histone deacetylase activity; 10 μg total proteins) in the absence or presence of 50 μM or 100 μM luteolin or 100 μM Trichostatin A (used as positive control of HDAC inhibition) for 6 or 24 h. After incubation with anti-acetyl HRP antibody for 1 h and washing, the level of acetylation of the substrate was detected at 450 nm on an ELISA plate reader. The experiments were repeated in triplicates. For Western blotting anti-acetylated H3 (K14) or H4 (K5) (Millipore/Upstate, USA) were used.

2.6. Wound healing migration assay

LNM35 cells were grown in six-well tissue culture dishes until confluence. Cultures were incubated for 10 min with Moscona buffer. A scrape was made through the confluent monolayer with a plastic pipette tip of 1 mm diameter. Afterwards, the dishes were washed twice and incubated at 37 °C in fresh RPMI containing 10% fetal calf serum in the presence or absence of the indicated concentrations of luteolin (1–10 μM). At the bottom side of each dish, two arbitrary places were marked where the width of the wound was measured with an inverted microscope (objective ×4). Wound closure was expressed as the average ± S.E.M of the difference between the measurements at time zero and the 2–24 h time period considered.

2.7. Matrigel, chick heart and Oris invasion assays

The invasiveness of the lung cancer cells LNM35 treated with luteolin (1 and 10 μM) was tested using BD Matrigel Invasion Chamber (8-μm pore size; BD Biosciences). Cells (1×10^5 cells in 0.5 mL of media and the indicated concentration of luteolin) were seeded into the upper chambers of the system, the bottom wells in the system were filled with RPMI supplemented with 10% fetal bovine serum as a chemo-attractant and then incubated at 37 °C for 24 h. Non-penetrating cells were removed from the upper surface of the filter with a cotton swab. Cells that have migrated through the Matrigel were fixed with 4% formaldehyde, stained with DAPI and counted in 25 random fields under a microscope. For quantification, the assay was carried out in duplicate and repeated three times.

For chick heart invasion assays, a drop of MCF-7/6, LNM35 or HepG2 cell suspensions was confronted overnight on top of semi-solid agar medium with precultured heart fragments (diameter 0.4 mm) isolated from 9-day-old chick embryos. Suspension cultures were treated with luteolin (1–10 μM) for 8 days in 1.5 ml culture medium, in a gyratory shaker at 120 rpm under a controlled atmosphere containing 10% CO_2 in air. Cells were fixed in Bouin–Hollande's solution and embedded in paraffin for histologic determination of cell invasiveness. Consecutive sections were stained with haematoxilin–eosin. For each experimental condition, at least two confrontations were examined. Invasion was scored as follows: grade 0, only heart tissue is found and no confronting cells can be observed; grade 1, the confronting test cells are attached to the precultured heart fragments and do not occupy the heart tissue; grade 2, occupation of the precultured heart fragments is limited to the outer fibroblast-like and myoblast cell layers; grade 3, the confronting cells have occupied the precultured heart fragments, but have left more than half of the original amount of heart tissue intact; grade 4, the confronting cells have occupied more than half of the original volume of the precultured heart fragments.

The Oris™ Cell Invasion Assay (AMS Biotechnology, Abingdon, UK) was used to investigate the impact of luteolin on LNM35, MCF7/6 and MDA-MB-231-1833 cell invasion *in vitro* within a 3-dimensional extracellular matrix comprised of a basement membrane extract (BME) of the murine Engelbreth–Holm–Swarm tumor. Cells were seeded at 100,000 cells/well and allowed to attach overnight onto plates coated with BME solution. Once the cells formed a confluent monolayer, the silicone stoppers were removed and the cells treated with luteolin (1 and 10 μM). Following 48 h invasion, cells were labeled with Calcein AM (Invitrogen), and images were acquired, in the absence of the mask, by use of an Olympus fluorescence microscope.

2.8. Tumor growth assay

Six-week-old athymic NMRI female nude mice (nu/nu, Elevage Janvier, France) were housed in filtered-air laminar flow cabinets and handled under aseptic conditions. Procedures involving animals and their care were conducted in conformity with Institutional guidelines that are in compliance with the Faculty of Medicine & Health Sciences, national and international laws and policies (EEC Council Directive 86/609, OJ L 358, 1, December 12, 1987; and NIH Guide for Care and Use of Laboratory Animals, NIH Publication No. 85-23, 1985). LNM35 cells (1×10^6 cells) were injected subcutaneously into the lateral flank of the nude mice. One week after inoculation, when tumors had reached the volume of approximately 100 mm^3, animals (six in each group) were treated for 18 days with luteolin (20 mg/kg/day, ip) or carrier solution. Tumor dimensions were measured with calipers every 3 days. Tumor volume (V) was calculated using the formula: $\mathbf{V}=0.4\times\mathbf{a}\times\mathbf{b}^2$, with "**a**" being the length and "**b**" the width of the tumor. After sacrifice, the tumors were excised and weighed.

2.9. Statistical analysis

Results were expressed as means ± S.E.M. The difference between experimental and control values was assessed by ANOVA followed by Dunnett post-hoc multiple comparison test. Tumour growth was analyzed using the unpaired Student's t-test. $P<0.05$ indicates a significant difference.

3. Results

3.1. Effect of luteolin on cell viability, apoptosis, and caspase-3/7 activation

As shown in Fig. 1, exposure of LNM35, HT29, HepG2, MCF7/6 and MDA-MB231-1833 cells to luteolin (1–200 μM) for 24 h decreased cellular viability in a concentration-dependent manner. The IC_{50} concentrations at 24 h were approximately 65, 60, and 90 μM for LNM35, HepG2, and MCF7/6 respectively, and more than 200 μM for

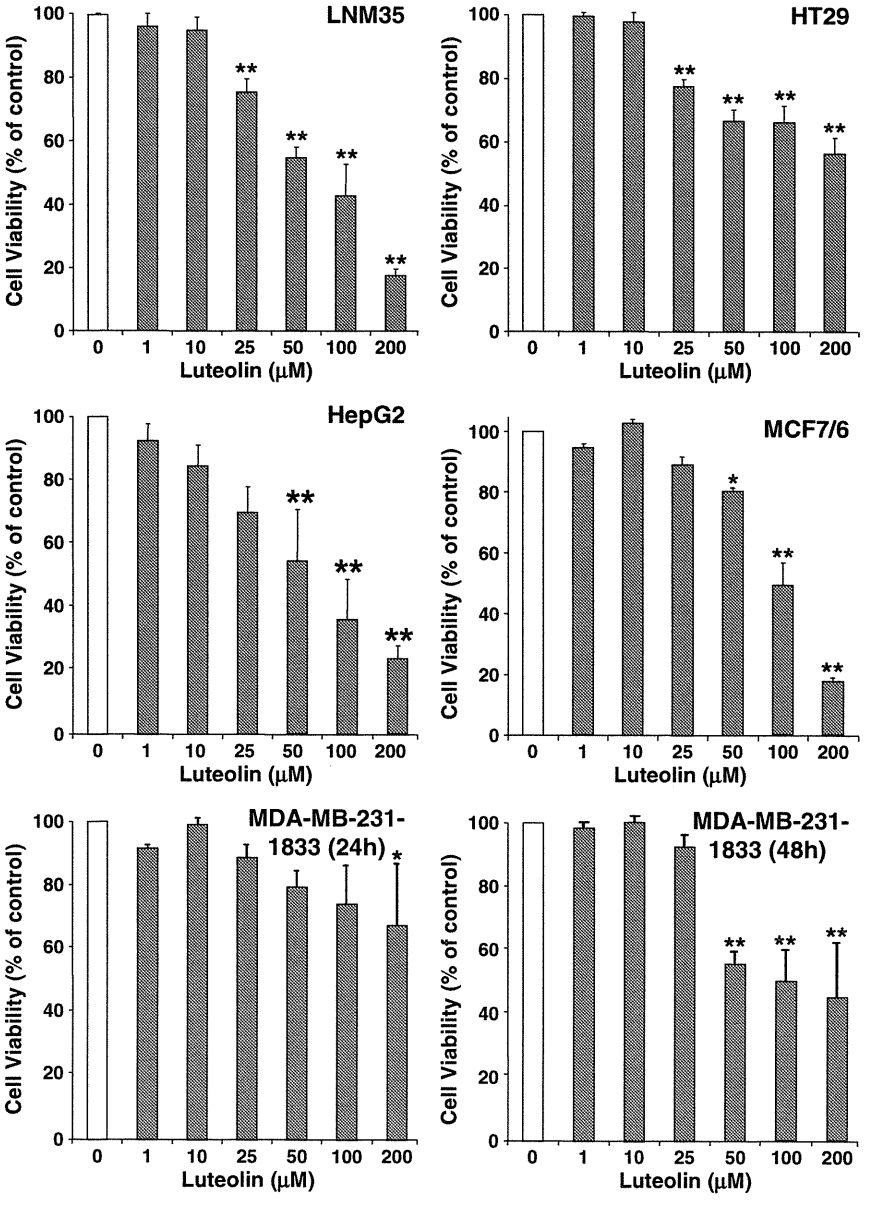

Fig. 1. Inhibition of cellular viability by luteolin. Exponentially growing LNM35, HT29, HepG2, MCF7/6 and MDA-MB231-1833 cells were treated for 24 h with vehicle (0.1% DMSO) or the indicated concentrations of luteolin and their viability was evaluated. All experiments were repeated at least three times. *Columns*, mean; *bars*, S.E.M. *Significantly different at $P<0.05$, **Significantly different at $P<0.01$.

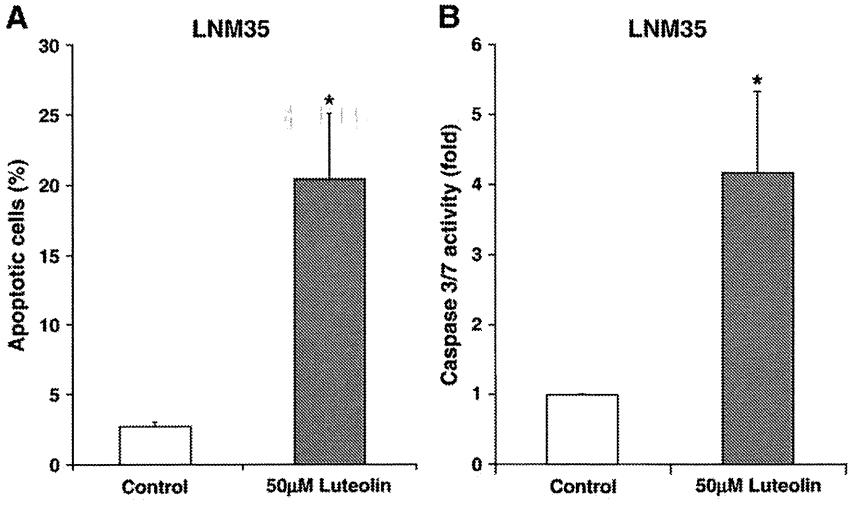

Fig. 2. Induction of caspase-mediated apoptosis by luteolin. Human lung cancer LNM35 cells were treated for 24 h with vehicle (0.1% DMSO) or 50 μM luteolin. A) LNM35 cells were treated with luteolin and then grown in fresh medium for the determination of sub-G1 fraction by fluorescence-activated cell sorting analysis. B) Induction of caspase-3/7 activity by luteolin was determined using the Caspase-Glo 3/7 Assay. The relative caspase 3/7 activity was normalized to the number of cells per well and expressed as fold induction compared with the control group. *Significantly different at $P<0.05$.

HT29, and MDA-MB231-1833 cells. LNM35 cells showed the highest sensitivity to the cytotoxic effects of luteolin, and death of all cells was observed after 48 h with 100 μM luteolin (not shown).

FACS analysis was performed to determine whether the effect of luteolin was due to apoptosis. Treatment of LNM35 cells for 24 h with 50 μM luteolin was associated with induction of apoptosis from 3.4% (for control 0.1% DMSO) to 20.4% for luteolin-treated cells (Fig. 2, left). These results suggest that LNM35 cells underwent apoptosis upon treatment with luteolin. Activation of caspase-3 is a penultimate step in apoptotic cell death pathways. The relative activity of caspases 3/7 was analyzed in LNM35 cells treated for 24 h with 50 μM luteolin, and normalized to the number of cells per well. As shown in Fig. 2 (right), caspase 3/7 activity increased 4-fold in LNM35 cells treated with luteolin ($P<0.05$).

3.2. Luteolin impairs cancer cell invasion

Cancer progression is associated with abrogation of the normal controls that limit cell migration and invasion, eventually leading to metastasis. The ability of luteolin to reduce cellular migration was investigated using a classic *in vitro* wound healing model. Luteolin was found to be effective in reducing cellular migration in the LNM35 cells in a dose- and time-dependent manner. However, this inhibition was not statistically significant (Fig. 3A). Most interestingly, luteolin impaired the invasion of LNM35 cells in Matrigel invasion assay (Fig. 3B). The inhibition of migration and Matrigel invasion seen following exposure of cells to low concentrations of luteolin (1 and 10 μM) occurred without reduction of cell viability (Fig. 1). Next, the invasiveness of LNM35, HepG2 and MCF-7/6 cancer cell lines was assessed in the chick heart invasion model (Fig. 3C). Histologic analysis of confronting cultures between LNM35, HepG2 and MCF-7/6 cancer cell aggregates and precultured heart fragments revealed that only MCF-7/6 cells spontaneously invaded into the chick heart tissue whereas no cellular adhesion or invasiveness could be observed in the chick heart fragments with the LNM35 (Nguyen et al., 2006) or HepG2 cells (data not shown). The effect of luteolin on invasion of MCF-7/6 cells into chick heart fragments was examined after 8 days of incubation. Fig. 3C shows that 1 μM luteolin slightly reduced the invasion of MCF-7/6 cell into the heart tissue (grade 3). At 10 μM luteolin, only a few MCF-7/6 cells could be observed in or around the heart tissue (grade 2). The abrogation of the MCF-7/6 invasive potential by 10 μM luteolin in chick heart fragments occurred in the absence of any detectable toxic effect on the heart tissue, confirming the specificity of the effect towards the cancer cells. Finally, we

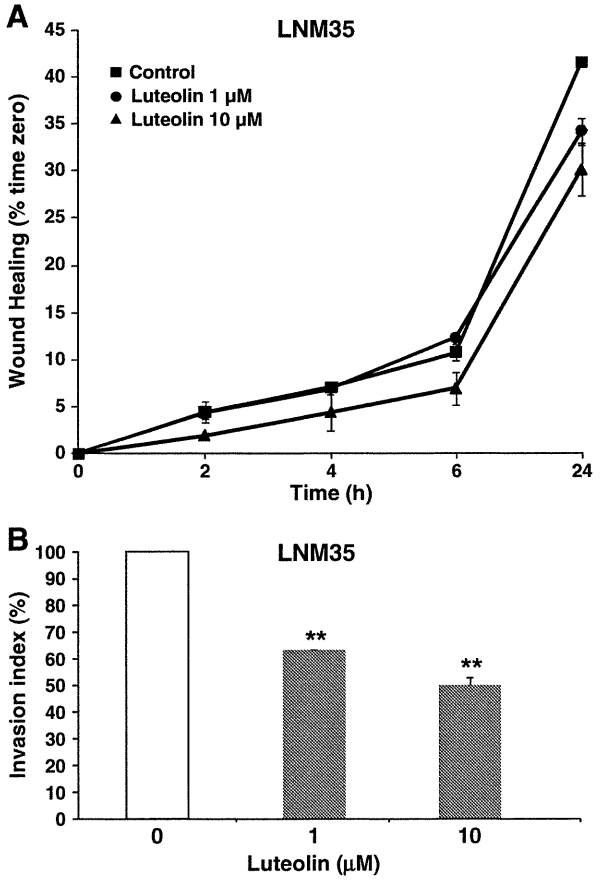

Fig. 3. Dose–response effect of luteolin on cellular migration and invasion. A) Wounds were introduced in LNM35 confluent monolayers cultured in the presence or absence (control) of luteolin (1 and 10 μM). The mean distance that cells travelled from the edge of the scraped area for 2, 4, 6 and 24 h at 37 °C was measured in a blinded fashion, using an inverted microscope (4× magnifications). Data are means ± S.E.M of two independent experiments. B) LNM35 cells were incubated for 24 h in the presence or absence of luteolin (1 and 10 μM). Cells that invaded into Matrigel were scored. *Columns*, mean; bars, S.E.M. C) Effect of luteolin on the penetration of MCF-7/6 breast cancer cells into cultured embryonic heart fragments. A representative experiment showing the invasion of MCF-7/6 cells cultured for 8 days into the host tissue in the presence or absence (control) of luteolin (1 and 10 μM) is presented. Light micrographs of paraffin sections stained with H&E. D) MDA-MB-213-1833 cells were incubated for 48 h in the presence or absence of luteolin (1 and 10 μM) onto an Oris cell invasion assay plate. Cell invasion images were acquired by fluorescence microscope.

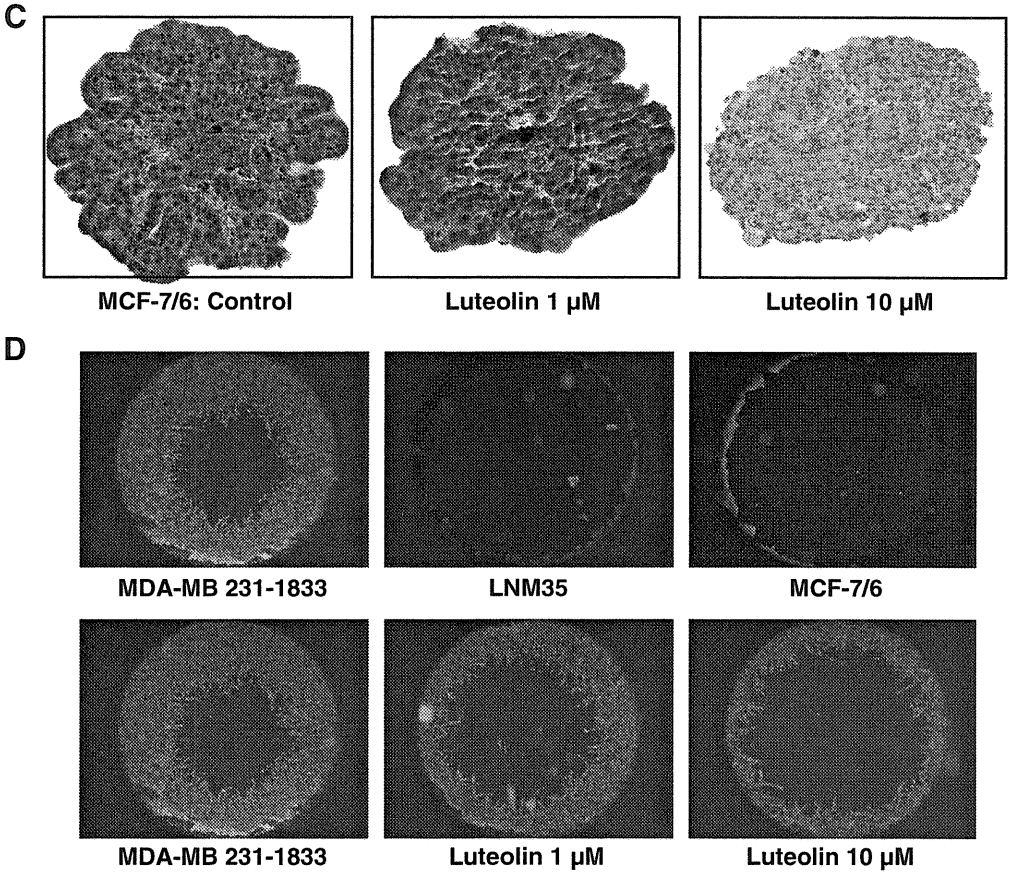

Fig. 3 (*continued*).

investigated the effect of 1 and 10 μM luteolin on the invasiveness of the LNM35, MCF-7/6 and MDA-MB231-1833 cells using Oris invasion assay. In this system, LNM35 and MCF-7/6 cells are not invasive in contrast to the highly invasive MDA-MB231-1833 clone (Fig. 3C). Again, luteolin reduced the invasiveness of these cells in a concentration-dependent manner (Fig. 3C). We can conclude that luteolin significantly reduced the invasive potential of lung cancer- (LNM35) and breast cancer-derived cells (MCF-7/6 and MDA-MB231-1833) cells.

3.3. Effect of luteolin on tumor growth and on cisplatin anticancer activity

The anticancer activity of luteolin was investigated in athymic mice inoculated with highly tumorigenic LNM35 human lung cancer cells. As shown in Fig. 4A, intraperitoneal administration of luteolin reduced the growth of LNM35 human tumor xenografts by 46% at day 18. Treatment with 20 mg/kg/day was well tolerated by the mice. There was no loss of body weight or other manifest sign of toxicity following luteolin administration. Our data encouraged us to investigate the potential of luteolin to enhance the cytotoxicity of cisplatin on LNM35 cells *in vitro* (Fig. 4B). Interestingly, low concentrations of luteolin (10 μM) potentiated the cytotoxic effect of cisplatin (25 μM) as shown in Fig. 4B.

3.4. Luteolin inhibits HDAC activity and induces acetylation of histones H3 and H4

In this study, we have examined the *in vitro* HDAC inhibitory effect of luteolin, resulting in an increased histone acetylation in cells. Using an *in vitro* HDAC assay, we have found that incubation of acetyl-conjugated H3 or H4 with HeLa nuclear extracts, which is a rich source of HDACs, completely abolished the H3 or H4 acetylation levels (Fig. 5, left panels, light grey bar). The addition of 100 μM of either luteolin (thin dashed bar) or TSA (positive control, dark grey bar) for 6 h, but not 50 μM luteolin (thick dashed bar), significantly inhibited HDAC activities present in the HeLa nuclear extract on both H3 and H4-acetylated substrates and resulted in a recovery of the acetylation levels. In other words, the HDAC inhibition is detected by an increase in the acetylation levels. Thus, addition of 100 μM luteolin for 6 h to H3-acetylated substrates and HeLa nuclear extract inhibited HDAC activity to a similar extent (18-20% inhibition), as the positive control (100 μM TSA) (Fig. 5, upper panel, left). This HDAC inhibitory effect was more pronounced on the acetyl-conjugated H4 compared to the acetyl-conjugated H3. The HDAC inhibition of the acetyl-conjugated H4 was about 30% and 50% upon the addition of 100 μM of luteolin or TSA, respectively (lower panel, left). In contrast, 50 μM of luteolin had no effect on acetylated H4. However, 24 h incubation resulted in an inhibition of HDAC activity even at 50 μM luteolin as shown by the increase in the acetylation levels (thick dashed bars) with both H3 and H4-acetylated. This HDAC inhibitory effect was about 30% with 50 μM and 80% with 100 μM luteolin on H3 acetyl-conjugated substrates (upper panel, left). Less pronounced, but still significant was the inhibition of HDAC detected when acetyl-conjugated H4 was used as a substrate (lower panel, left) within 24 h incubation. Thus, addition of luteolin inhibited both H3 and H4 HDAC activities in HeLa nuclear extracts.

Finally, we investigated the effect of 50 and 100 μM luteolin on the H3 and H4 histone acetylation levels using western blot analysis and selective antibodies directed against acetylated histones H3 (K14) and H4 (K5). As shown in Fig. 5 (right panels), luteolin clearly increased

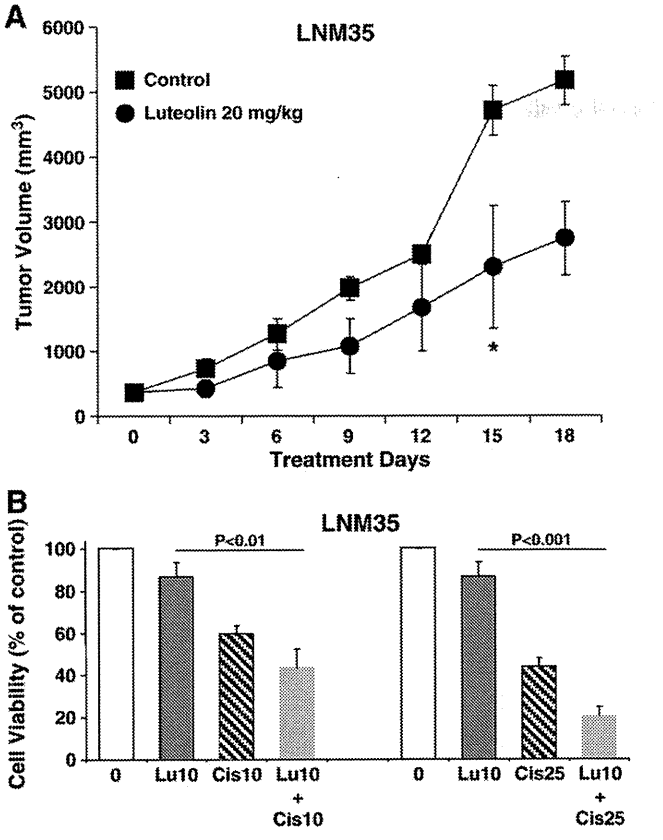

Fig. 4. Impact of luteolin on the tumorigenicity and toxicity of cisplatin in human lung LNM35 tumor xenografts and on monolayers. A) Nude mice were xenografted subcutaneously with human lung LNM35 cancer cells (10^6 cells per animal) and treated with luteolin (20 mg/kg/day, intraperitoneal injections) or control carrier solution alone, for 18 days. Data points represent the means ± S.E.M of 6 to 7 mice per group. *Significantly different at $P<0.05$. B) LNM35 cells were incubated in the presence or absence of luteolin (10 μM), cisplatin (10–25 μM) or with combined luteolin (10 μM) and cisplatin (10–25 μM) treatment for 24 h. Cell viability was measured. All experiments were repeated at least three times. *Columns*, mean; *bars*, S.E.M.

the acetylation levels of histones H3 and H4 upon 24 h treatment, especially at the higher concentration (100 μM). This increase is consistent with the *in vitro* HDAC assay shown in the left panels. Taken together, these findings provide biochemical and molecular evidence for the potential of luteolin as a novel HDAC inhibitor.

4. Discussion

Luteolin (3′,4′,5,7-tetrahydroxyflavone), a member of the flavonoid family found in various fruits and vegetables, including carrots, peppers, celery, olive oil, peppermint, thyme, rosemary and oregano, exhibits a diverse repertoire of pharmacological actions, including anti-inflammatory, antioxidant, antimicrobial and anti-proliferative effects (Chiu and Lin, 2008). A potent anticancer effect has already been shown for luteolin in several studies. Luteolin is probably also a safe molecule for potential clinical use in cancer therapy.

In the present study, we have presented several cellular and molecular mechanisms supporting the antitumor effects of luteolin in a series of human cancer cells originating from lung, breast, colon, and liver tumors. These are i) luteolin cytotoxicity through inhibition of cancer cell survival and induction of apoptosis associated with robust caspase-3 and -7 activation; ii) inhibition of cancer cell invasion in the Matrigel, chick heart fragments and Oris assays; iii) HDAC inhibition by luteolin, suggesting that this dietary flavonoid play important roles in gene expression and tumor regulation; iv) inhibition of Akt activation by luteolin in LNM35 cells in a time- and concentration-dependent manner (Unpublished data); v) cooperation of luteolin with the DNA damaging agent cisplatin to induce additive toxicity in cancer cells in vitro; and vi) antitumor activity against LMN35 cancer cell xenografts in vivo.

We demonstrate that intraperitoneal administration of luteolin (20 mg/kg) as a single agent for 3 weeks reduced LNM35 tumor growth by 46%. Our findings are in agreement with other animal studies showing that luteolin is able to diminish the growth of tumor xenografts induced by prostate cancer cells LNCaP, HAK-1B hepatoma cells, and LLC Lewis lung carcinoma cells (Chiu and Lin, 2008; Kim et al., 2006; Selvendiran et al., 2006). In contrast, luteolin (40 mg/kg body weight) alone failed to reduce the growth of the HCT116 tumors, but reinforced the effect of cisplatin (Shi et al., 2007). Cisplatin is a major chemotherapeutic agent for the treatment of bladder, ovarian and lung cancers (Ferraldeschi et al., 2007). The mechanism of action of cisplatin involves covalent binding to purine DNA bases, which leads primarily to cellular apoptosis. However, in the present study the anticancer effect of luteolin is mainly due to the inhibition of histone deacetylase. It is plausible; therefore, that luteolin and cisplatin in combination exert additive or synergistic cytotoxic and antitumor responses in cancer cells through interplay between the components of the DNA damage and repair signaling pathways and gene expression linked to apoptosis. Consistent with this statement, our study demonstrates that luteolin potentiates the growth inhibitory effect of cisplatin on LNM35 lung cancer cells *in vitro* so that co-treatment with cisplatin and luteolin is an option that is worthy of further investigation *in vivo*.

As well as the effect on cell viability, we also investigated other cancer cell-related dysfunctions such as migration and invasion. A recent study indicates that luteolin (5–40 μM) exerts inhibitory effects on HGF-induced HepG2 hepatoma cell migration and invasion of Matrigel in Boyden chemotaxis chambers probably through the suppression of the c-Met receptor as well as ERK1/2 and Akt phosphorylation (Lee et al., 2006). In the present study we provide evidence that luteolin, in concentrations that are not cytotoxic to the cells, exert an inhibitory effect on the invasive phenotype of LNM35 and MCF7/6 and MDA-MB231-1833 cancer cells. We hypothesize; therefore, that luteolin is able to counter both the locally invasive and metastasizing behaviour of tumor cells. As metastasis is the major cause of death in cancer patients, the development of new treatment regimens that reduce tumor dissemination is highly important in cancer therapy.

Earlier reports showed that luteolin sensitized cancer cells to therapeutic cytotoxic agents through suppression of critical survival pathways, including phosphatidylinositol 3′-kinase (PI3K)/Akt, nuclear factor kappa B (NF-κB), STAT3, as well as through stimulation of apoptosis and cell death pathways mediated by the p53 tumor suppressor (Bagli et al., 2004; Ju et al., 2007; Lee et al., 2005; Selvendiran et al., 2006; Shi et al., 2007; Xavier et al., 2009). Recently, it has been demonstrated that peroxiredoxin and prohibitin, which are implicated in ROS metabolism and apoptosis, are associated with the anticancer effects of luteolin (Yoo et al., 2009), and that protein kinase Cε and c-Src are targets of luteolin (Byun et al., 2010).

The levels of histone acetylation/deacetylation play important regulatory roles in gene expression and tumor progression. This is accomplished by the actions of histone acetyltrasferases (HATs), which acetylate the lysine residues in core histones leading to a more transcriptionally active chromatin, and by histone deacetylases (HDACs), which remove the acetyl groups from the lysine residues leading to the formation of a transcriptionally silenced chromatin (Selvi and Kundu, 2009; Shahbazian and Grunstein, 2007; Thiagalingam et al., 2003; Yang and Seto, 2007). Inhibition of HDACs can thus result in hyperacetylation of histones and increased transcriptional activity. Consequently, HDAC inhibitors have emerged as important molecules that can reverse gene silencing. They modulate a wide variety of cellular functions, including cell differentiation, cell cycle progression, apoptosis, and angiogenesis. Many HDAC inhibitors have

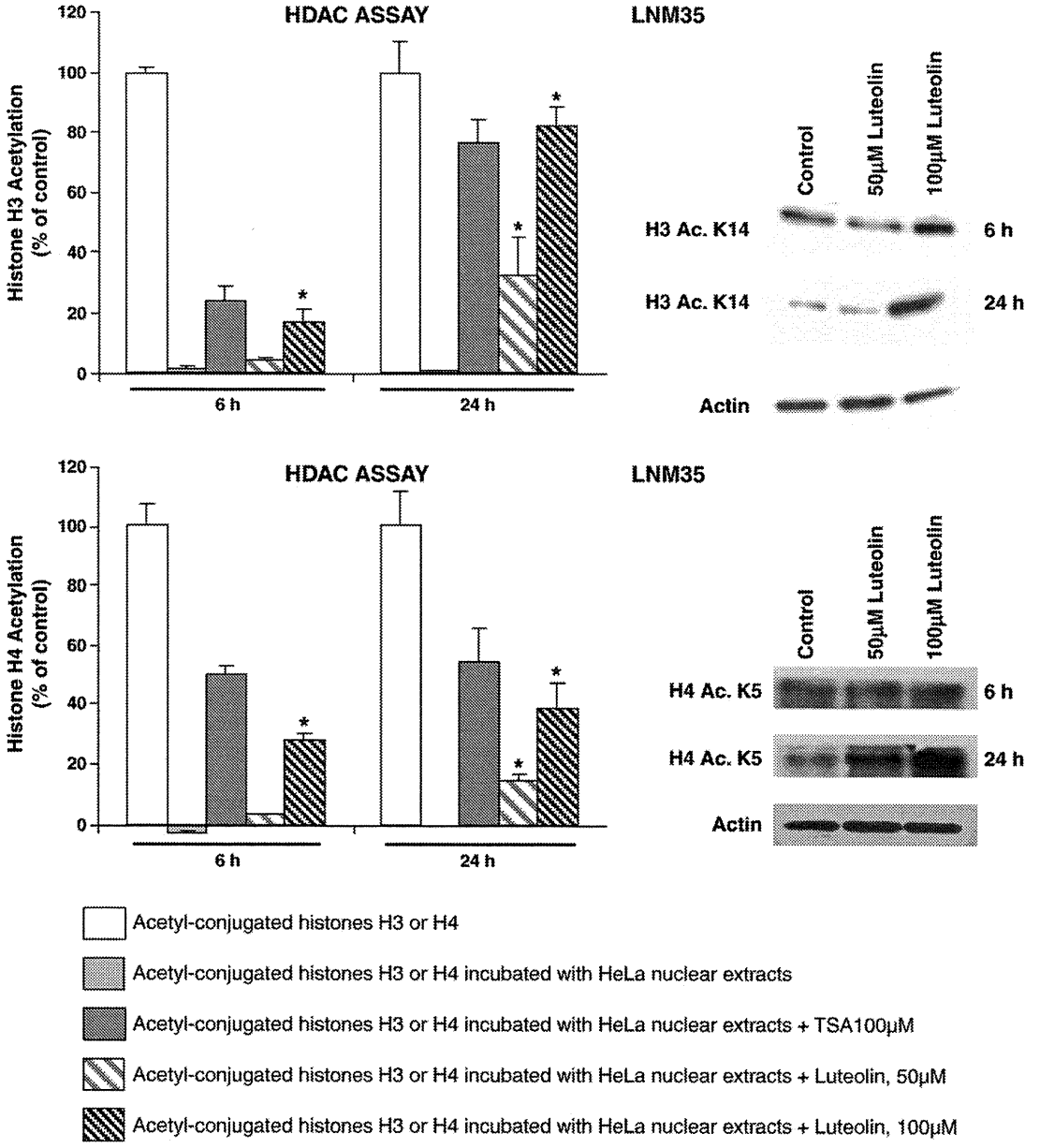

Fig. 5. The effects of luteolin on histone deacetylase activities and H3 and H4 acetylation levels. Left panels: HeLa nuclear extract was added to acetyl-conjugated histone H3 and H4 peptides and incubated for 6 or 24 h with vehicle (0.1% DMSO), TSA (100 μM), or luteolin (50 or 100 μM) as indicated. The HDAC assay was performed. The data were normalized to the level of acetyl-conjugated histones H3 or H4 (white bars). Asterisks indicate significant difference ($P<0.05$). Right panels: LNM35 cells were treated for 6 and 24 h with vehicle (0.1% DMSO as control) and the indicated concentrations of luteolin. Histones H3 and H4 acetylation levels were detected by western blot analysis using the acetylated H3 (K14) and H4 (K5) antibodies, respectively. Actin was used as a control for equal protein loading.

shown promise as potential chemopreventive agents in *in vitro* studies as well as in animal models (Al-Janadi et al., 2008; Balasubramanian et al., 2009; Drummond et al., 2005; Monneret, 2007; Santini et al., 2007; Witt and Lindemann, 2009). In addition, some of these HDAC inhibitors such as suberoylanilide hydroxamic acic (SAHA), valproic acid, and depsipeptide are currently being tested as anticancer agents in clinical trials and show promising results in patients with leukaemias and solid tumors (Luu et al., 2008; Munster et al., 2009). There are now 11 HDAC inhibitors in clinical trial, including inhibitors with a broad spectrum of HDAC isoforms as well as inhibitors with isoform selectivity. However, the exact mechanism by which HDAC inhibitors cause cell death is still unclear and the specific roles of individual HDAC enzymes as therapeutic targets have not yet been established. A very recently published article demonstrates that the inhibition of histone deacetylases slows down replication forks, activates dormant origins, and induces DNA damage (Conti et al., 2010). In this study, we show for the first time that luteolin is a potent HDAC inhibitor *in vitro* targeting the acetylation of histones H3 and H4. These results are in line with other studies demonstrating that luteolin binds to both histones H3 and H4 (Shoulars et al., 2005). Further studies are needed to determine whether luteolin is a selective or a general HDCA inhibitor.

It has been demonstrated that histone deacetylase inhibitors require caspase activity to induce apoptosis in lung and prostate carcinoma cells (Sonnemann et al., 2006). This might explain the link between the HDAC inhibitory activity of luteolin, the activation of caspase 3/7 and its ability to induce cell death. We suggest that luteolin inhibits histone deacetylases, which can then lead to the activation of caspase 3/7 causing DNA fragmentation and cell death.

This could also occur through a more indirect pathway where HDAC inhibition leads to increased acetylation levels, which in turn may also lead to activation of various genes including caspases.

In conclusion, our data indicate that luteolin induced cancer cell death at least in part *via* caspase-3/7-dependent mechanisms. We also found that luteolin exerts potent histone deacetylase inhibition and growth inhibition of highly aggressive LNM35 human lung cancer xenografts in nude mice. Furthermore, luteolin is able to sensitize LNM35 cancer cells to the cytotoxic effects of the DNA damaging agent cisplatin and to reduce the invasiveness of cancer cells.

Further investigations using the LNM35 xenografts model are warranted to determine the therapeutic potential of luteolin, other flavonoids and recognized histone deacetylase inhibitors in the management of lung cancer, in combination with the standard anticancer drug cisplatin, or other agents targeting DNA integrity or oncogenic signaling pathways involved in cancer cell survival and tumor angiogenesis.

Acknowledgements

This work was financially supported by the Research Affairs at the UAE University under contracts no. 01-04-8-11/08, and 01-03-8-12/05. This work was also partly supported by the Terry Fox Fund for Cancer Research under project no. 2006-02 Terry Fox UAE, Emirates Foundation Research Grant no. 2009/80, INSERM funds and a Geconcerteerde Onderzoeks Actie from the Ghent University (GOA nr. 01G01307). The funders had no role in the study design, data collection and analysis, decision to publish, or preparation of the manuscript. Special thanks to Dr. Jan Mester for drafting this manuscript. We thank Prof. Joan Massague from Howard Hughes Medical Institute for providing the MDA-MB-213-1833 cell line.

References

Al-Janadi, A., Chandana, S.R., Conley, B.A., 2008. Histone deacetylation : an attractive target for cancer therapy? Drugs R.D. 9, 369–383.

Bagli, E., Stefaniotou, M., Morbidelli, L., Ziche, M., Psillas, K., Murphy, C., Fotsis, T., 2004. Luteolin inhibits vascular endothelial growth factor-induced angiogenesis; inhibition of endothelial cell survival and proliferation by targeting phosphatidylinositol 3′-kinase activity. Cancer Res. 64, 7936–7946.

Balasubramanian, S., Verner, E., Buggy, J.J., 2009. Isoform-specific histone deacetylase inhibitors: the next step. Cancer Lett. 280, 211–221.

Byun, S., Lee, K.W., Jung, S.K., Lee, E.J., Hwang, M.K., Lim, S.H., Bode, A.M., Lee, H.J., Dong, Z., 2010. Luteolin inhibits protein kinase C(epsilon) and c-Src activities and UVB-induced skin cancer. Cancer Res 70, 2415–2423.

Chiu, F.L., Lin, J.K., 2008. Downregulation of androgen receptor expression by luteolin causes inhibition of cell proliferation and induction of apoptosis in human prostate cancer cells and xenografts. Prostate 68, 61–71.

Conti, C., Leo, E., Eichler, G.S., Sordet, O., Martin, M.M., Fan, A., Aladjem, M.I., Pommier, Y., 2010. Inhibition of histone deacetylase in cancer cells slows down replication forks, activates dormant origins, and induces DNA damage. Cancer Res. 70, 4470–4480.

Coseri, S., 2009. Natural products and their analogues as efficient anticancer drugs. Mini-Rev. Med. Chem. 9, 560–571.

Drummond, D.C., Noble, C.O., Kirpotin, D.B., Guo, Z., Scott, G.K., Benz, C.C., 2005. Clinical development of histone deacetylase inhibitors as anticancer agents. Annu. Rev. Pharmacol. Toxicol. 45, 495–528.

Ferraldeschi, R., Baka, S., Jyoti, B., Faivre-Finn, C., Thatcher, N., Lorigan, P., 2007. Modern management of small-cell lung cancer. Drugs 67, 2135–2152.

Ju, W., Wang, X., Shi, H., Chen, W., Belinsky, S.A., Lin, Y., 2007. A critical role of luteolin-induced reactive oxygen species in blockage of tumor necrosis factor-activated nuclear factor-kappaB pathway and sensitization of apoptosis in lung cancer cells. Mol. Pharmacol. 71, 1381–1388.

Kim, J.H., Lee, E.O., Lee, H.J., Ku, J.S., Lee, M.H., Yang, D.C., Kim, S.H., 2006. Caspase activation and extracellular signal-regulated kinase/Akt inhibition were involved in luteolin-induced apoptosis in Lewis lung carcinoma cells. Ann. NY Acad. Sci. 1090, 147–160.

Kozaki, K., Miyaishi, O., Tsukamoto, T., Tatematsu, Y., Hida, T., Takahashi, T., 2000. Establishment and characterization of a human lung cancer cell line NCI-H460-LNM35 with consistent lymphogenous metastasis via both subcutaneous and orthotopic propagation. Cancer Res. 60, 2535–2540.

Lee, H.J., Wang, C.J., Kuo, H.C., Chou, F.P., Jean, L.F., Tseng, T.H., 2005. Induction apoptosis of luteolin in human hepatoma HepG2 cells involving mitochondria translocation of Bax/Bak and activation of JNK. Toxicol. Appl. Pharmacol. 203, 124–131.

Lee, W.J., Wu, L.F., Chen, W.K., Wang, C.J., Tseng, T.H., 2006. Inhibitory effect of luteolin on hepatocyte growth factor/scatter factor-induced HepG2 cell invasion involving both MAPK/ERKs and PI3K-Akt pathways. Chem. Biol. Interact. 160, 123–133.

Luu, T.H., Morgan, R.J., Leong, L., Lim, D., McNamara, M., Portnow, J., Frankel, P., Smith, D.D., Doroshow, J.H., Wong, C., Aparicio, A., Gandara, D.R., Somlo, G., 2008. A phase II trial of vorinostat (suberoylanilide hydroxamic acid) in metastatic breast cancer: a California Cancer Consortium study. Clin. Cancer Res. 14, 7138–7142.

Monneret, C., 2007. Histone deacetylase inhibitors for epigenetic therapy of cancer. Anticancer Drugs 18, 363–370.

Munster, P., Marchion, D., Bicaku, E., Lacevic, M., Kim, J., Centeno, B., Daud, A., Neuger, A., Minton, S., Sullivan, D., 2009. Clinical and biological effects of valproic acid as a histone deacetylase inhibitor on tumor and surrogate tissues: phase I/II trial of valproic acid and epirubicin/FEC. Clin. Cancer Res. 15, 2488–2496.

Nguyen, Q.D., Rodrigues, S., Rodrigue, C.M., Rivat, C., Grijelmo, C., Bruyneel, E., Emami, S., Attoub, S., Gespach, C., 2006. Inhibition of vascular endothelial growth factor (VEGF)-165 and semaphorin 3A-mediated cellular invasion and tumor growth by the VEGF signaling inhibitor ZD4190 in human colon cancer cells and xenografts. Mol. Cancer Ther. 5, 2070–2077.

Parkin, D.M., Bray, F., Ferlay, J., Pisani, P., 2005. Global cancer statistics, 2002. CA Cancer J. Clin. 55, 74–108.

Ross, J.A., Kasum, C.M., 2002. Dietary flavonoids: bioavailability, metabolic effects, and safety. Annu. Rev. Nutr. 22, 19–34.

Santini, V., Gozzini, A., Ferrari, G., 2007. Histone deacetylase inhibitors: molecular and biological activity as a premise to clinical application. Curr. Drug Metab. 8, 383–393.

Selvendiran, K., Koga, H., Ueno, T., Yoshida, T., Maeyama, M., Torimura, T., Yano, H., Kojiro, M., Sata, M., 2006. Luteolin promotes degradation in signal transducer and activator of transcription 3 in human hepatoma cells: an implication for the antitumor potential of flavonoids. Cancer Res. 66, 4826–4834.

Selvi, R.B., Kundu, T.K., 2009. Reversible acetylation of chromatin: implication in regulation of gene expression, disease and therapeutics. Biotechnol. J. 4, 375–390.

Shahbazian, M.D., Grunstein, M., 2007. Functions of site-specific histone acetylation and deacetylation. Annu. Rev. Biochem. 76, 75–100.

Shi, R., Huang, Q., Zhu, X., Ong, Y.B., Zhao, B., Lu, J., Ong, C.N., Shen, H.M., 2007. Luteolin sensitizes the anticancer effect of cisplatin via c-Jun NH2-terminal kinase-mediated p53 phosphorylation and stabilization. Mol. Cancer Ther. 6, 1338–1347.

Shoulars, K., Rodrigues, M.A., Crowley, J.R., Turk, J., Thompson, T., Markaverich, B.M., 2005. Nuclear type II [3H]estradiol binding sites: a histone H3–H4 complex. J. Steroid Biochem. Mol. Biol. 96, 19–30.

Sonnemann, J., Hartwig, M., Plath, A., Saravana Kumar, K., Müller, C., Beck, J., 2006. Histone deacetylase inhibitors require caspase activity to induce apoptosis in lung and prostate carcinoma cells. Cancer Lett. 232, 148–160.

Strick, R., Strissel, P.L., Borgers, S., Smith, S.L., Rowley, J.D., 2000. Dietary bioflavonoids induce cleavage in the MLL gene and may contribute to infant leukemia. Proc. Natl Acad. Sci. USA 97, 4790–4795.

Thiagalingam, S., Cheng, K.H., Lee, H.J., Mineva, N., Thiagalingam, A., Ponte, J.F., 2003. Histone deacetylases: unique players in shaping the epigenetic histone code. Ann. NY Acad. Sci. 983, 84–100.

Witt, O., Lindemann, R., 2009. HDAC inhibitors: magic bullets, dirty drugs or just another targeted therapy. Cancer Lett. 280, 123–124.

Xavier, C.P., Lima, C.F., Preto, A., Seruca, R., Fernandes-Ferreira, M., Pereira-Wilson, C., 2009. Luteolin, quercetin and ursolic acid are potent inhibitors of proliferation and inducers of apoptosis in both KRAS and BRAF mutated human colorectal cancer cells. Cancer Lett. 281, 162–170.

Yang, X.J., Seto, E., 2007. HATs and HDACs: from structure, function and regulation to novel strategies for therapy and prevention. Oncogene 26, 5310–5318.

Yoo, D.R., Jang, Y.H., Jeon, Y.K., Kim, J.Y., Jeon, W., Choi, Y.J., Nam, M.J., 2009. Proteomic identification of anti-cancer proteins in luteolin-treated human hepatoma Huh-7 cells. Cancer Lett. 282, 48–54.